

1 **Unchanged PM2.5 levels over Europe during COVID-19 were**  
2 **buffered by ammonia**

3

4 **Nikolaos Evangeliou<sup>1,\*</sup>, Ondřej Tichý<sup>2</sup>, Marit Svendby Otervik<sup>1</sup>, Sabine Eckhardt<sup>1</sup>, Yves**  
5 **Balkanski<sup>3</sup>, Didier [A. Hauglustaine](#)<sup>3</sup>**

6

7 <sup>1</sup> NILU, Department for Atmospheric & Climate Research (ATMOS), 2007 Kjeller, Norway.

8 <sup>2</sup> The Czech Academy of Sciences, Institute of Information Theory and Automation, Prague, Czech  
9 Republic.

10 <sup>3</sup> Laboratoire des Sciences du Climat et de l'Environnement (LSCE), CEA-CNRS-UVSQ, 91191,  
11 Gif-sur-Yvette, France.

12

13 \* Corresponding author: N. Evangeliou ([Nikolaos.Evangeliou@nilu.no](mailto:Nikolaos.Evangeliou@nilu.no))

14

15

16 **Abstract**

17 The coronavirus outbreak in 2020 had devastating impact on human life, albeit a positive effect  
18 for the environment reducing emissions of primary aerosols and trace gases and improving air quality.  
19 In this paper, we present inverse modelling estimates of ammonia emissions during the European  
20 lockdowns of 2020 based on satellite observations. Ammonia has a strong seasonal cycle and mainly  
21 originates from agriculture. We further show how changes in ammonia levels over Europe, in  
22 conjunction with decreases in traffic-related atmospheric constituents modulated PM2.5. The key  
23 result of this study is a -9.8% decrease in ammonia emissions in the first half of 2020 compared to  
24 the same period in 2016–2019 attributed to restrictions related to the global pandemic. We further  
25 calculate the delay in the evolution of the ammonia emissions in 2020 before, during and after  
26 lockdowns, by a sophisticated comparison of the evolution of ammonia emissions during the same  
27 time periods for the reference years (2016–2019). Our analysis demonstrates a clear delay in the  
28 evolution of ammonia emissions of -77 kt, that was mainly observed in the countries that suffered the  
29 strictest travel, social and working measures. Despite the general drop in emissions during the first  
30 half of 2020 and the delay in the evolution of the emissions during the lockdown period, satellite and  
31 ground-based observations showed that the European levels of ammonia increased. On one hand, this  
32 was due to the reduction of  $SO_2$  and  $NO_x$  (precursors of the atmospheric acids with which ammonia  
33 reacts) that caused less binding and thus less chemical removal of ammonia (smaller loss – higher  
34 lifetime); on the other, the majority of the emissions persisted, because ammonia mainly originates  
35 from agriculture, a primary production sector that was influenced slightly by the lockdown  
36 restrictions. Despite the projected drop in various atmospheric aerosols and trace gases, PM2.5 levels  
37 stayed unchanged or even increased in Europe, due to a number of reasons attributed to the  
38 complicated  $NH_3 - H_2SO_4 - HNO_3$  system. Higher water vapour during the European lockdowns  
39 favoured more sulfate production from  $SO_2$  and  $OH$  (gas phase) or  $O_3$  (aqueous phase). Ammonia  
40 first reacted with sulfuric acid, also producing sulfate. Then, the continuously accumulating free  
41 ammonia reacted with nitric acid shifting the equilibrium reaction towards particulate nitrate. In high  
42 free ammonia atmospheric conditions such as those in Europe during the 2020 lockdowns, a small  
43 reduction of  $NO_x$  levels drives faster oxidation toward nitrate and slower deposition of total inorganic  
44 nitrate causing high secondary PM2.5 levels.

45

Deleted: n

Deleted: not

Deleted: , as practically agricultural activity never ceased

Deleted: (due to higher atmospheric abundance)

## 50 1 Introduction

51 Ammonia (NH<sub>3</sub>), the most abundant gas, has played a vital role in the evolution of human  
52 population through the Haber–Bosch process (Chen et al., 2019). However, today it is recognized to  
53 have significant negative influence, not only for the environment (Stevens et al., 2010), but also for  
54 human population (Cohen et al., 2017; Pope and Dockery, 2006) and the climate (De Vries et al., 2011).  
55 As an alkaline molecule, ammonia regulates the pH of clouds, while its excessive atmospheric  
56 deposition and terrestrial runoff affect natural reservoirs creating algae blooms and degrading water  
57 quality (Camargo and Alonso, 2006; Krupa, 2003). When emitted to the atmosphere, it reacts with  
58 the abundant sulfuric and nitric acids (Malm, 2004) forming sulfate, nitrate, and ammonium and  
59 contributing up to 50% to the total aerosol mass (Anderson et al., 2003). The latter has implications  
60 for human health (Gu et al., 2014) as aerosols penetrate the human respiratory system and accumulate  
61 in the lungs (Pope III et al., 2002) causing premature mortality (Lelieveld et al., 2015). Furthermore,  
62 through secondary aerosol formation (Pozzer et al., 2017), ammonia has a significant impact (i) on  
63 regional climate (Bellouin et al., 2011) causing visibility problems and contributing to haze effect,  
64 and (ii) on global climate directly by scattering incoming radiation (Henze et al., 2012) and indirectly  
65 as cloud condensation nuclei (Abbatt et al., 2006) altering the Earth’s radiative balance.

66 The largest portion of atmospheric ammonia originates from the synthesis of nitrogen  
67 fertilizers, which are in high demand for agriculture (Erisman et al., 2007). The expansion of intensive  
68 agriculture during the 20<sup>th</sup> century has increased atmospheric ammonia above natural levels (Erisman  
69 et al., 2008), while the projected growth of the global population will likely create larger nutritional  
70 needs that are expected to further increase ammonia emissions during the 21<sup>st</sup> century (Pai et al.,  
71 2021). Other sources of ammonia include emissions from livestock (Sutton et al., 2000a), industry,  
72 ammonia-rich watersheds (Sørensen et al., 2003), traffic (Kean et al., 2009), sewage (Reche et al.,  
73 2012), humans (Sutton et al., 2000b), biomass and domestic combustion (Sutton et al., 2008; Fowler  
74 et al., 2004) and volcanic eruptions (Sutton et al., 2008).

75 In the past years, atmospheric ammonia observations were mostly limited to ground-based  
76 measurements with relatively sparse monitoring networks. This resulted in large emission  
77 uncertainties in regions poorly covered by measurements (Heald et al., 2012). Today, satellite  
78 products are capable to record daily ammonia column concentrations providing useful information  
79 on its atmospheric abundance. Recently, Van Damme et al. (2021) analyzed Infrared Atmospheric  
80 Sounding Interferometer (IASI) retrievals and showed increased ammonia levels over most of Europe  
81 after 2015. Then, suddenly the COVID-19 outbreak came in 2020 creating a unique situation  
82 (Baekgaard et al., 2020), which affected all segments of life in a detrimental way (Chakraborty and  
83 Maity, 2020; Sohrabi et al., 2020). As a measure to inhibit further spread of the virus, authorities took

84 strict social, travel and working restrictions for months, which resulted in lower traffic-related  
85 emissions and improved air quality (Bauwens et al., 2020; Dutheil et al., 2020; Sicard et al., 2020).  
86 Illustrating the impact on emissions, Guevara et al. (2021) reported average emission reductions in  
87 Europe to be 33% for  $NO_x$ , 8% for non-methane volatile organic compounds (NMVOCs), and 7%  
88 for  $SO_x$  during the strictest lockdowns in 2020, while more than 85% of the total reduction is  
89 attributed to road transport.  $CO_2$  emissions were also decreased by 11% over Europe during the first  
90 lockdowns (Diffenbaugh et al., 2020), so as aerosols did; notably Black Carbon (BC) emissions  
91 dropped by 11% (Evangelou et al., 2020) and Aerosol Optical Depth (AOD) decreased up to 20%  
92 over Central and Northern Europe (Acharya et al., 2021).

93 While the COVID-19 lockdown impact on emissions for primary aerosols and trace gases has  
94 been studied extensively, how ammonia emissions were affected in Europe is unknown. The latter is  
95 very important and may have largely moderated the atmospheric levels of particulate matter (Giani  
96 et al., 2020; Guevara et al., 2021; Matthias et al., 2021), because of ammonia's contribution to  
97 secondary PM<sub>2.5</sub> (particulate matter) formation (Anderson et al., 2003). Here, we make use of  
98 satellite measurements of ammonia and a novel inversion algorithm to track how ammonia emissions  
99 changed before, during and after the European lockdowns in 2020. We examine the reasons behind  
100 the estimated changes and validate the results against ground-based observations from the EMEP  
101 measurement network (<https://emep.int/mscw/>, **Figure S I**). Finally, we calculate the resulting impact  
102 of ammonia changes during the European lockdowns on the formation of PM<sub>2.5</sub> using a chemistry  
103 transport model (CTM) and try to interpret the mechanisms governing these changes.

## 104 2 Methods

### 105 2.1 Cross-Track Infrared Sounder (CrIS) ammonia measurements

106 The CrIS sensor onboard the NASA Suomi National Polar-orbiting Partnership provides  
107 atmospheric soundings at high spectral resolution (0.625  $cm^{-1}$ ) (Shephard et al., 2015) resulting in  
108 improved vertical sensitivity for ammonia at the surface (Zavvalov et al., 2013). The CrIS fast  
109 physical algorithm (Shephard and Cady-Pereira, 2015) retrieves ammonia at 14 vertical levels using  
110 a physics-based optimal estimation retrieval, which also provides the vertical sensitivity (averaging  
111 kernels) and an estimate of the retrieval errors (error covariance matrices) for each measurement.  
112 Shephard et al. (2020) reports a total column random measurement error of 10–15%, with total  
113 random errors of ~30%. The individual profile random errors are 10–30%, while total profile random  
114 errors increase above 60% due to the limited vertical resolution (Shephard et al., 2020). Vertical  
115 sensitivity and error calculations are also important when using CrIS observations in satellite inverse  
116 modelling applications (Li et al., 2019; Cao et al., 2020) as a satellite observational operator can be

117 generated in a robust manner (see next sections). The detection limit of CrIS measurements has been  
118 calculated down to 0.3–0.5 ppbv (Shephard et al., 2020) and the product has been validated  
119 extensively against ground-based observations (Dammers et al., 2017; Kharol et al., 2018) showing  
120 small differences and high correlations.

121 Daily CrIS ammonia satellite measurements (version 1.6.2) were gridded on  $0.5^\circ \times 0.5^\circ$  covering  
122 all Europe ( $10^\circ\text{W}$ – $50^\circ\text{E}$ ,  $25^\circ\text{N}$ – $75^\circ\text{N}$ ) from 1st January to 30th June 2020. [Data were screened prior](#)  
123 [to its use with Quality Flag  \$\geq 4\$ , as recommended in the CrIS documentation, and Cloud Flag  \$\neq 1\$ . The](#)  
124 [latter excludes retrievals that are performed under thin cloud conditions and are not as reliable as](#)  
125 [retrievals performed under cloud-free conditions \(White et al., 2023\)](#). Gridding was chosen to limit  
126 the large number of observations (around 10,000 per day per vertical level for 2550 retrievals January  
127 to June 2020), hence the need for a large number of source-receptor matrices (SRMs), which is  
128 computationally inefficient. Specifically, day and night-time observations from CrIS were averaged  
129 in each  $0.5^\circ$  resolution grid-cell daily from 1st January to 30th June 2020. This gridding method,  
130 although simple, it gives more robust results than classic interpolation methods and presents small  
131 standard deviations of the gridded values (see Tichý et al., 2023). Sitwell and Shephard (2021)  
132 showed that the averaging kernels of CrIS ammonia are significant only for the lowest six levels (the  
133 upper eight have no influence into the satellite observations) and therefore we have considered these  
134 six vertical levels ( $\sim 1018$ – $619$  hPa).

## 135 2.2 Source-receptor matrix (SRM) calculations

136 SRMs were calculated for each  $0.5^\circ \times 0.5^\circ$  grid-cell over Europe ( $10^\circ\text{W}$ – $50^\circ\text{E}$ ,  $25^\circ\text{N}$ – $75^\circ\text{N}$ )  
137 using the Lagrangian particle dispersion model FLEXPART version 10.4 (Pisso et al., 2019) adapted  
138 to model ammonia. The model releases computational particles that are tracked backward in time  
139 using hourly ERA5 (Hersbach et al., 2020) assimilated meteorological analyses from the European  
140 Centre for Medium-Range Weather Forecasts (ECMWF) with 137 vertical layers and a horizontal  
141 resolution of  $0.5^\circ \times 0.5^\circ$ . FLEXPART simulates turbulence ([Cassiani et al., 2015](#)), unresolved  
142 mesoscale motions (Stohl et al., 2005) and convection (Forster et al., 2007). SRMs were calculated  
143 for 7 days backward in time, at temporal intervals that matched satellite measurements and at spatial  
144 resolution of  $0.5^\circ \times 0.5^\circ$ . This 7-day backward tracking is sufficiently long to include almost all  
145 ammonia sources that contribute to surface concentrations at the receptors given a typical atmospheric  
146 lifetime of about a day (Evangelidou et al., 2021; Van Damme et al., 2018).

147 The complicated heterogeneous chemistry of ammonia was modelled with the Eulerian model  
148 LMDz-OR-INCA, which couples the LMDz (Laboratoire de Météorologie Dynamique) General  
149 Circulation Model (GCM) (Hourdin et al., 2006) with the INCA (INteraction with Chemistry and  
150 Aerosols) model (Folberth et al., 2006; Hauglustaine et al., 2004) and with the land surface dynamical

Deleted: (Cassiani et al., 2014)

Field Code Changed

152 vegetation model ORCHIDEE (ORganizing Carbon and Hydrology In Dynamic Ecosystems)  
153 (Krinner et al., 2005). The model has a horizontal resolution of  $2.5^{\circ} \times 1.3^{\circ}$ , and 39 hybrid vertical  
154 levels extending to the stratosphere. It accounts for large-scale advection of tracers (Hourdin and  
155 Armengaud, 1999), deep convection (Emanuel, 1991), while turbulent mixing in the planetary  
156 boundary layer (PBL) is based on a local second-order closure formalism. The model simulates  
157 atmospheric transport of natural and anthropogenic aerosols and accounts for emissions, transport  
158 (resolved and sub-grid scale), and dry and wet (in-cloud/below-cloud scavenging) deposition of  
159 chemical species and aerosols interactively. LMDz-OR-INCA includes a full chemical scheme for  
160 the ammonia cycle and nitrate particle formation, as well as a state-of-the-art  
161  $\text{CH}_4/\text{NO}_x/\text{CO}/\text{NMHC}/\text{O}_3$  tropospheric photochemistry (Hauglustaine et al., 2014). The global  
162 transport of ammonia was simulated for 2020 with a month of spin-up by nudging the winds of the  
163 3-hourly ERA5 (Hersbach et al., 2020) with a relaxation time of 10 days (Hourdin et al., 2006).

164 For the calculation of ammonia's lifetime, LMDz-OR-INCA ran with traditional emissions for  
165 anthropogenic, biomass burning and oceanic emission sources from ECLIPSEv5 (Evaluating the  
166 CLimate and Air Quality ImPacts of Short-livEd Pollutants), GFED4 (Global Fire Emission Dataset)  
167 and GEIA (Global Emissions InitiAtive) (hereafter called "EGG") (Bouwman et al., 1997; Giglio et  
168 al., 2013; Klimont et al., 2017). FLEXPART uses the exponential mass removal for radioactive  
169 species based on the e-folding lifetime (Pisso et al., 2019), which gives the time needed to reduce the  
170 species mass to  $1/e$  contribution. We calculated the e-folding lifetime (Kristiansen et al., 2016; Croft  
171 et al., 2014) of ammonia from LMDz-OR-INCA, assuming that the loss occurs as a result of all  
172 processes affecting ammonia (chemical reactions, deposition) with a minimum time-step of 1800 s.  
173 Then we calculated the exponential loss of ammonia and the respective loss-rate constant  $\kappa$  ( $\text{s}^{-1}$ ). We  
174 point to Tichý et al. (2023) for more details on the methodology to avoid repetition.

175 Ammonia has a complicated atmospheric chemistry and may react with sulfuric and nitric acid  
176 producing sulfate and nitrate. However, under certain atmospheric conditions, the equilibrium  
177 reaction with nitric acid can be shifted to the left producing free ammonia (Seinfeld and Pandis, 2000).  
178 Tichý et al. (2023) showed that production of free ammonia happened very rarely in continental  
179 Europe in 2013–2020 period. Nevertheless, we have previously published a full validation of the  
180 obtained CTM concentrations against all the available ground-based measurements of ammonia  
181 globally (Tichý et al., 2023), from the EMEP network (<https://emep.int/mscw/>) in Europe, EANET  
182 (East Asia acid deposition NETwork) in Southeastern Asia (<https://www.eanet.asia/>) and AMoN  
183 (Ammonia Monitoring Network in the US, AMoN-US; National Air Pollution Surveillance Program  
184 (NAPS) sites in Canada) in North America (<http://nadp.slh.wisc.edu/data/AMoN/>).

185 **2.3 Inverse modelling of ammonia emissions**

186 The proposed inversion method is based on a comparison of the CrIS satellite observations with  
 187 the model profile retrievals to estimate the spatiotemporal ammonia emissions. The comparison of  
 188 remote-sense observations such as CrIS with model (or in-situ) profiles is not straightforward as in  
 189 the cases of ground-based observations. Here, we used the more rigorous approach of the “instrument  
 190 operator” (see equation below), after interpolation of the model profile to the first six levels of the  
 191 satellite product (Rodgers, 2000):

192 
$$\ln(v^{ret}) = \ln(v^a) + A(\ln(v^{true}) - \ln(v^a)) \quad Eq. 1$$

193 where  $v^{ret}$  is the retrieved profile concentration vector,  $v^a$  is a priori profile concentration vector,  
 194  $v^{true}$  is the true profile concentration vector, and  $A$  is the averaging kernel matrix in logarithmic  
 195 space (for each  $0.5^\circ \times 0.5^\circ$  resolution grid-cell). In our inversion setup, we directly compared the  
 196 retrieved  $v^{ret}$  and the observed satellite column concentration  $v^{sat}$  that is given by CrIS. In our case,  
 197  $v^{true}$  is equal to the modelled concentration  $v^{mod}$  calculated from the SRMs and a prior emission  
 198 inventory. The argument for this approach is that  $v^{ret}$  is what the satellite would observe if  $v^{mod}$  was  
 199 the true profile. This is a useful technique for evaluating if the retrieval algorithm is performing as  
 200 designed, i.e., is it unbiased and the calculated root mean square error (RMSE) is within the expected  
 201 variability. Further details about the algorithm and the setup can be found in Tichý et al. (2023).

202 The goal of the inversion is to iteratively update prior emissions by minimizing the distance  
 203 between  $v^{sat}$  and  $v^{ret}$  by correcting the emission flux  $x$  in the term  $v^{mod} = srm^{Flex} x^a$  ( $srm^{Flex}$   
 204 denotes the FLEXPART SRMs), at each grid-cell and each of the six vertical levels that are important  
 205 for CrIS (Sitwell et al., 2022):

206 
$$\arg \min_{x^a \rightarrow x} \|v^{sat} - v^{ret}\|_2^2 \quad Eq. 2$$

207 The inverse problem is constructed for each spatial element of the computational domain.  
 208 Inspired by the construction of covariance matrix in Cao et al. (2020), we consider  $4^\circ$  surroundings  
 209 (445 km), expressed by the index set  $\mathbb{S}$ , of which the column concentrations are considered due to  
 210 computational effectivity. Note that we observed low sensitivity of resulting emission estimates to  
 211 this choice. Then, we can formulate the inverse problem for each spatial element as:

212 
$$[v_{s_i}^{sat}; s_i \in \mathbb{S}] = [v_{s_i}^{ret}; s_i \in \mathbb{S}] q^{\mathbb{S}} \quad Eq. 3$$

213 where the left side of the equation is formed by the vector with aggregated CrIS observations, vectors  
 214  $v_{s_i}^{ret}$  form a block-diagonal matrix, and  $q^{\mathbb{S}}$  is an unknown vector with correction coefficients for each  
 215 temporal element of the emission. The inverse problem in Eq. 3 was solved using the least squares  
 216 with adaptive prior covariance (LS-APC) algorithm (Tichý et al., 2016). The algorithm is based on a

217 Bayesian model which assumes that all coefficients are positive and that the abrupt changes in their  
218 neighbouring values are less probable. It is shown that the method is less sensible to manual tuning  
219 of regularization parameters (see sensitivity tests in Tichý et al. (2020)) than classical optimization  
220 procedures, which is crucial for such a large dataset where each spatial element represents a separate  
221 inverse problem.

222 A detailed description of the algorithm is given in Tichý et al. (2016). Here, we do not describe  
223 the algorithm again but explain a few modifications that were necessary for this study. By estimating  
224 the correction coefficients  $q^s$  for each grid-cell of the spatial domain (10°W–50°E, 25°N–75°N), we  
225 can propagate the coefficients through Eq. 2 to update a priori emissions  $x^a$  in the model  
226 concentration term  $v^{mod}$ . We follow Li et al. (2019) and Cao et al. (2020) to bound the ratio between  
227 the prior and the posterior emissions. The lower and upper bound of this ratio is set to 0.01 and 100,  
228 respectively, to omit the unrealistically low or high emissions. We consider these bounds large  
229 enough to allow for new emission sources to be exposed, not presented in the prior emissions.

230 We evaluate the performance of the inversion by using three a priori emission datasets, (i) one  
231 based on Van Damme et al. (2018) calculations (Evangelou et al., 2021) (hereafter denoted as “VD”),  
232 (ii) the ECLIPSEv6 inventory (Klimont, 2022; Klimont et al., 2017) (combined with biomass burning  
233 emissions from GFEDv4 (Giglio et al., 2013)) as the most recent one (denoted as “EC6G4”), and (iii)  
234 the average of four emission inventories for ammonia, except for these two mentioned before, “EGG”  
235 (see previous section), and “NE” calculated from IASI (Infrared Atmospheric Sounding  
236 Interferometer) observation (Evangelou et al., 2021) (denoted as “avgEENV”). To account for the  
237 spatiotemporal impact of the lockdown on the European emissions, we corrected prior emission  
238 inventories of ammonia (EGG, EC6G4 and avgEENV) for 2020 using adjustment factors (AFs)  
239 adopted from Doumbia et al. (2021). The same was done for  $SO_2$  and  $NO_x$  (precursors of sulfuric and  
240 nitric acid in the atmosphere) in EGG that was used to calculate ammonia’s loss rates using LMDz-  
241 OR-INCA model (see section 2.2). This dataset provides, for the January–August 2020 period,  
242 gridded AFs at a  $0.1^\circ \times 0.1^\circ$  resolution on a daily resolution for transportation (road, air and ship  
243 traffic), power generation, industry and residential sectors. The quantification of AFs is based on  
244 activity data collected from different databases and previously published studies. These emission AFs  
245 have been applied to the CAMS global inventory, and the changes in emissions of the main pollutants  
246 have been assessed for different regions of the world in the first 6 months of 2020 (Doumbia et al.,  
247 2021).

248 **Figure 1** shows the comparison of prior and posterior concentrations against independent  
249 observations (observations that were not used in the inversion algorithm) from the EMEP network  
250 (<https://emep.int/mscw/>, **Figure S 1**) for January–July 2020. Note that prior concentrations of



251 ammonia result by coupling the FLEXPART SRMs with prior emissions (from VD, ECLIPSEv6 and  
 252 avgEENV), while posterior concentrations by coupling the SRMs with the calculated posterior  
 253 emissions. In **Figure 1** it is evident that the most accurate reconstruction of surface concentrations  
 254 with respect to the EMEP observations was obtained using avgEENV as the a priori information, and  
 255 therefore the results presented hereafter are based on this setup. We performed inversions for the first  
 256 half of 2020 to assess the effect of lockdown measures on ammonia emissions, as well as the situation  
 257 after lockdown measures were taken away (rebound period). To have a more generic view, we also  
 258 performed inverse modelling calculations for the first half of each year between 2016–2019 (reference  
 259 period). Then, we assess in impact of ammonia changes on aerosol formation (PM2.5), by feeding  
 260 the posterior emissions to the LMDz-OR-INCA model and calculating the production of PM2.5.

## 261 2.4 Statistical tests

262 To evaluate the comparisons between modelled and observed concentrations of ammonia, we  
 263 used the root mean squared logarithmic error (RMSLE) defined as follows:

$$264 \quad RMSE = \sqrt{\frac{\sum_{i=1}^N (C_m - C_o)^2}{N}} \quad \text{and} \quad RMSLE = \sqrt{\frac{1}{N} \sum_{i=1}^N (\log C_m - \log C_o)^2} \quad Eq. 4$$

265 where  $C_m$  and  $C_o$  are the modelled and measured ammonia concentrations and  $N$  is the total number  
 266 of observations. The commonly used squared Pearson correlation coefficient ( $r$ ) was also used as a  
 267 measure of linear correlation between two sets of data defined as:

$$268 \quad r = \frac{\sum (C_m - \bar{C}_m)(C_o - \bar{C}_o)}{\sqrt{(\sum (C_m - \bar{C}_m)^2)(\sum (C_o - \bar{C}_o)^2)}} \quad Eq. 5$$

269 where the distance of modelled and measured ammonia concentrations from the mean ( $\bar{C}_m$  and  $\bar{C}_o$ ) is  
 270 computed. Finally, the standard deviation was adopted as a measure of the dispersion of modelled  
 271 ammonia from the observations, which is the true value:

$$272 \quad \sigma = \sqrt{\frac{\sum (C_m - \bar{C}_m)^2}{N}} \quad Eq. 6$$

273 The mean fractional bias ( $MFB$ ) was selected as a symmetric performance indicator that gives equal  
 274 weights to under- or over-estimated concentrations (minimum to maximum values range from -200%  
 275 to 200%). It was used in the independent validation (validation against measurements that were  
 276 excluded from the inversion, see section 3.3) of the posterior concentrations of ammonia during the  
 277 European lockdowns of 2020 and is defined as:

$$278 \quad MFB = \frac{1}{N} \frac{\sum_{i=1}^N (C_m - C_o)}{\sum_{i=1}^N \left(\frac{C_m + C_o}{2}\right)} \quad Eq. 7$$

279 For the same reason, the mean absolute error was computed normalized (*nMAE*) over the average of  
280 all the actual values (observations here), which is a widely used simple measure of error:

281 
$$MAE = \frac{\sum_{i=1}^N |C_m - C_o|}{\sum_{i=1}^N C_o} \quad Eq. 8$$

## 282 3 Results

### 283 3.1 Emission changes of ammonia due to COVID-19 restrictions over Europe

284 The reason behind the selected three priors used in the inversion (EGG, EC6G4 and avgEENV)  
285 of ammonia is trifold; (i) they are based on the most recent estimates, (ii) they present different spatial  
286 distribution, and (iii) they were derived using different methodologies. More specifically, EC6G4 is  
287 based on the emission model GAINS (Klimont et al., 2017), while VD uses satellite observations  
288 combined with a box model (Evangelidou et al., 2021). As mentioned in the previous section, it is seen  
289 that the most accurate representation of surface model concentrations was achieved using the  
290 avgEENV a priori, which forces posterior concentrations closer to 1×1 line, whereas the obtained  
291 statistics are significantly better than using other priors (**Figure 1**). Therefore, the results presented  
292 below have all been obtained using avgEENV as the prior emission dataset keeping results using the  
293 other two priors in the Supplements.

294 The total prior emissions of ammonia over Europe for the inversion period (January – June),  
295 the posterior emissions for years 2016–2019 and the posterior emissions during the lockdown year  
296 2020 (January – June) are plotted in **Figure 2** (the results from inversions using EC6G4 and VD prior  
297 emissions are illustrated in **Figure S 2** and **S 3**). The total prior ammonia emitted between January  
298 and June in Europe were equal to 1061 kt (**Figure 2a**). To check whether calculated changes in 2020  
299 were due to meteorology and avoid misinterpretation of our findings, inverse calculations of ammonia  
300 were performed for the reference years 2016–2019 (January–June) using respective observations  
301 from CrIS and exactly the same set-up as the one described in section 2 (Methods). The total posterior  
302 emissions of ammonia over Europe for the reference period (2016 – 2019) were estimated to be  
303 1665±330 kt (4-y mean±SD) or 57% higher than the prior (**Figure 2b**). Finally, for January–June  
304 2020 the derived emission estimates were equal to 1568±172 kt (posterior±uncertainty) (**Figure 2c**).  
305 This is 48% higher than the prior and 6% lower than the posterior emissions of January–June 2016–  
306 2019.

307 The weekly-average evolution of prior and posterior emissions of ammonia over Europe  
308 (January to June) for 2016–2019 show a similar pattern with small year-to-year variability (**Figure**  
309 **2d,e**), and similar temperatures (**Figure S 4**) thus insignificant impact from the prevailing

Formatted: Font: (Default) Times New Roman, 12 pt, Bold,  
Font colour: Text 1, English (UK)

310 meteorology that would justify change in emissions due to volatilisation. The weekly posterior  
 311 ammonia emissions over Europe changed during the lockdown period (2020) as compared to the  
 312 reference years (**Figure 2f**). Satellites and national monitoring measurements of ammonia show that  
 313 emissions peak in spring (March) and late-summer in Europe (Van Damme et al., 2022)  
 314 corresponding to the two main fertilization periods (Paulot et al., 2014). Ammonia abundances are  
 315 however high throughout the entire spring–summer period due to agriculture associated with rising  
 316 temperature (Sutton et al., 2013). Ammonia posterior emissions in 2020 declined by -9.8% as  
 317 compared to the same period over the previous four years (2016–2019, **Figure 2f**). Although the  
 318 obtained posterior emissions for the reference period (dashed grey line and shade) are very similar to  
 319 those of 2020, (solid blue line and shade in Figure 2f), emissions during lockdown period in 2020  
 320 dropped substantially, outside of the deviation of the emissions in the reference period (Figure 2f).

- Deleted: agricultural
- Deleted: activities and
- Deleted: dependent volatilization of ammonia
- Deleted: Interestingly, the posterior ammonia emissions in the first half of 2020 were insensitive to the meteorological conditions. ...
- Deleted: with respect to annual variance
- Deleted: grey shade
- Deleted: levels and trend (dashed grey line),
- Deleted: variance
- Deleted: calculated for
- Deleted: bottom blue line,

### 3.2 Uncertainty of the posterior emissions

322 As described in section 2.3 in more detail, we considered 4° surroundings of each spatial  
 323 element of our inversion domain from which the CrIS observations were used in the inverse problem.  
 324 This means that 45 spatial elements in CrIS space were used, with six vertical levels each, for each  
 325 of the 26 temporal emission elements. To calculate the associated uncertainty of the posterior  
 326 estimates, we tested two sources of uncertainty: (i) how different surroundings for each spatial  
 327 element affect posterior emissions of ammonia and (ii) how the use of different prior emissions affects  
 328 posterior ammonia. We organized a series of sensitivity tests using surroundings covering 2°, 3° and  
 329 4° from each grid-cell. This selection is realistic as it was shown previously in Cao et al. (2020) for  
 330 the construction of prior emission error covariance matrix. For the second source of uncertainty, we  
 331 performed the same inversion using not only EC6G4 and VD priors, but also adding results using two  
 332 more datasets for ammonia (in total four), which have 10 times higher emissions, namely EGG and  
 333 NE (see section 2.3).

334 The calculated absolute uncertainties are depicted in **Figure 3a–c** together with the relative  
 335 uncertainty (**Figure 3d**) with respect to the posterior emissions of ammonia (posterior ammonia is  
 336 shown in **Figure 2c**). The first source of uncertainty (different surroundings) slightly affects the  
 337 resulting posterior emissions of ammonia (**Figure 3a**) causing an average relative uncertainty below  
 338 4% in the European emissions. The second source of uncertainty (use of different priors) causes much  
 339 larger bias as shown in **Figure 3b** (average relative uncertainty 35%). The reason for this is obviously  
 340 the large variation of the EGG (Bouwman et al., 1997; Giglio et al., 2013; Klimont et al., 2017) and  
 341 NE (Evangelidou et al., 2021) prior datasets that have total emissions in the first half of 2020 of 63.5  
 342 and 53.3 Tg, respectively, in contrast to only 6.2 and 5.7 Tg for EC6G4 and VD. Hence, the results  
 343 presented here are sensitive to the use of prior emission dataset. The modelled concentrations (that  
 344 replaces the hypothetical true column concentration in Eq. 1) is calculated by the SRMs and the prior

- Deleted: **Figure 5**
- Formatted: Font: (Default) Times New Roman, 12 pt, Bold
- Formatted: Indent: First line: 1.25 cm, Space After: 0 pt, Adjust space between Latin and Asian text, Adjust space between Asian text and numbers
- Deleted: **Figure 5**
- Formatted: Font: (Default) Times New Roman, 12 pt, Bold
- Deleted: **Figure 5**
- Formatted: Font: (Default) Times New Roman, 12 pt, Bold
- Deleted: **Figure 5**
- Formatted: Font: (Default) Times New Roman, 12 pt, Bold

361 emission and, therefore, play a key role in the comparison of the CrIS value ( $v^{sat}$ ) and retrieved value  
362 ( $v^{ret}$ ) (see Eq. 2). Also, the modelled concentrations stand as the argument of the natural logarithm  
363 weighted by the averaging kernel in logarithmic space. The linearization of this operator as suggested  
364 by Sitwell and Shephard (2021) may reduce the dependency on the prior emission term, however,  
365 this is beyond the scope of this study. Overall, the propagated (absolute and relative) uncertainties of  
366 the posterior emissions are shown in **Figure 3c** and **d** and are equal to 11% over Europe on average  
367 (**Figure 3**). The latter shows that our calculations are robust on one hand, but dependent on the use  
368 of a priori information on the other.

Deleted: **Figure 5**

Formatted: Font: (Default) Times New Roman, 12 pt, Bold

Deleted: **Figure 5**

Formatted: Font: (Default) Times New Roman, 12 pt, Bold

Deleted: ¶

### 369 3.3 Validation of posterior ammonia against independent measurements

370 The optimized emissions of ammonia must be validated against independent observations,  
371 because the inversion algorithm has been designed to reduce the model–observation mismatches.  
372 Here, the reduction of the posterior concentration differences from the observations from CrIS is  
373 determined by the weighting that is given to the observations and, hence, such comparison depends  
374 on this weighting (dependent observations). Therefore, the ideal comparison of any posterior  
375 emission resulting from top-down methods would be against measurements that were not included in  
376 the inversion algorithm (independent observations). Here, we used ground-based observations of  
377 ammonia from all EMEP sites (<https://emep.int/mscw/>) for the period of our study as an independent  
378 dataset for validation. All stations are illustrated in **Figure S 1**.

379 As we mentioned in section 2.3, we evaluated the efficiency of the inversion and the most  
380 effective a priori dataset for our purpose by assessing the match between the calculated posterior  
381 concentrations against all the available observations from EMEP (N=3957) for the study period  
382 (**Figure 1**). More specifically, after it became evident that the most accurate results were obtained  
383 with avgEENV as the prior (relationship closer to unity against measured ammonia), we saw an  
384 immediate improvement in the statistical tests used (nRMSE, nMAE and RMSLE) when using the  
385 posterior emissions to model ammonia in FLEXPART during the first half of 2020 (**Figure 1** – right  
386 panel). nMAE decreased from 0.80 using the prior emissions to 0.76 using the posterior ones,  
387 accordingly nRMSE of the posterior concentrations dropped to 0.073 as compared to -0.069 using  
388 the prior emissions, while the RMSLE decreased from 0.60 using prior emissions to 0.55 using the  
389 optimized a posteriori emissions. To get a better insight on how modelled concentrations improved  
390 towards ammonia observations, eight random EMEP stations were selected to show timeseries of  
391 prior and posterior concentrations in the first half of 2020 (**Figure S 5**). Although large peaks were  
392 not reproduced, all statistics were improved using the posterior emissions of ammonia.

Deleted: are

397 **3.4 Country-level changes due to COVID-19 restrictions**

398 To document the emission changes of ammonia over the different European countries before,  
399 during and after the 2020 lockdowns, we report the weekly evolution of the emissions for 16 countries  
400 individually (**Figure 4**). Specifically, weekly emissions were averaged for each country based on  
401 respective country definitions that are shown in **Figure S 6** using the avgEENV prior.

402 Most countries show that ammonia emissions declined or at least stayed less affected by the  
403 2020 lockdowns, as compared to the same period during the reference years (2016–2019). Countries  
404 with substantial decreases in the 2020 lockdown emissions were The Netherlands (-16%) and  
405 Belgium (-23%), both countries with important agricultural activity, as well as Denmark (-20%),  
406 Ireland (-18%) and Ukraine (-18%). Smaller changes were recorded in Spain (-2.1%), Czechia (-  
407 4.0%) and Italy (-6.0%) despite the intensive lockdown measures. This practically shows that  
408 agricultural activity is insignificantly affected, even in periods of extraordinary austerity, as the last  
409 remaining primary production sector, necessary for human life.

410 We note that the largest emissions of ammonia in European countries were seen around  
411 March–April (weeks 8–16) and in summer. These coincide with the fertilization periods mentioned  
412 previously (Paulot et al., 2014) that control the seasonality of ammonia’s emissions. In most European  
413 countries, the time of the year when fertilizers can be applied is tightly regulated (Ge et al., 2020). In  
414 the Netherlands and Belgium, for instance, the largest ammonia contributing region in Europe,  
415 application of nitrogen fertilizer is only allowed from February to mid-September. This produces two  
416 peak periods, in March and late May (**Figure 4**). Manure application also follows stringent  
417 regulations and is only allowed in the same periods depending on the type of manure (slurry or solid)  
418 and the type of land (grassland or arable land) (Van Damme et al., 2022).

419 To understand and position where ammonia emissions changed during the European  
420 lockdowns of 2020, we plot the difference of the posterior emissions of ammonia during the lockdown  
421 period (15 March – 30 April) for the same period in **Figure 5a**. We calculate higher emissions of  
422 ammonia during the lockdown of +115 kt as compared to the prior emissions. Note that inversion  
423 algorithms aim at reducing the mismatches between modelled concentrations and observations (in  
424 our case, from CrIS satellite measurements) by correcting emissions. This means that different  
425 posterior emissions are most likely, due to errors in the prior emissions and do not indicate any impact  
426 from the restriction measures.

427 Therefore, we demonstrate the impact of the COVID-19 lockdowns over Europe in 2020, by  
428 calculating the emission anomaly for the lockdown period from 2016–2020 (same period as the 2020  
429 lockdowns, namely 15 March – 30 April) in **Figure 5b**. Emissions during the 2020 lockdowns

**Deleted:** .  
**Deleted:** Like in the previous section, the country-based emissions were calculated for

**Deleted:** never stopped  
**Deleted:** agriculture is

**Deleted:** or

**Deleted:** In Belgium, nitrogen fertilizers are only allowed between mid-February and end of August (Van Damme et al., 2022), therefore the peaks in early March and summer (**Figure 3**). Accordingly, in Germany, it is also restricted in winter months and depends on fertilizer type and land type (Kuhn, 2017), while restrictions during the same months are applied in the US (Paulot et al., 2014).

**Deleted:** The largest differences can be seen in Spain, Romania and North Italy.

445 dropped by -29 kt with respect to the same period in 2016 – 2020 showing the impact of the COVID-  
446 19 restrictions. Maximum decreases were seen in The Netherlands and Belgium, both countries  
447 [comprising high emissions](#) (**Figure 5b**) that also suffered heavily from the COVID-19 outbreak  
448 (Bendz and Aaberge, 2020) and took strict lockdown measures. Other areas where [significant](#) changes  
449 were calculated were Northern Italy, Switzerland and Austria, while Scandinavian countries were not  
450 affected. This agrees well with the state of the epidemic in these countries in spring 2020. While  
451 North Italy was the first country outside China to suffer high mortality rates and, thus, dramatic social  
452 restrictions in spring 2020, Norway, Sweden, Denmark and Finland showed total infected cases far  
453 below 1% per capita, mostly suffering higher rates later in 2020 (Gordon et al., 2021).

454 [As mentioned previously](#), ammonia emissions increase in spring (March) and late-summer in  
455 Europe ([Van Damme et al., 2022; Paulot et al., 2014](#)). Therefore, calculating the difference in the  
456 calculated emissions during the lockdown from the period before or after is practically meaningless  
457 and cannot show the lockdown impact since agricultural activity [was slightly affected in 2020](#). For  
458 this reason we quantify the delay in the evolution of the [2020](#) emissions by calculating emission  
459 differences in the lockdowns from the period before (Lock – Prelock) for the lockdown year 2020  
460 and emission differences (Lock – Prelock) for the reference years (2016 – 2019). Then, we plot their  
461 spatial differences in **Figure 5c**. Accordingly, we do the same calculation for differences in the  
462 rebound period (the period after the restrictions were relaxed) from the lockdown period (Rebound –  
463 Lock) in 2020 and compare them with Rebound – Lock for the reference years 2016 – 2019 (**Figure**  
464 **5d**). We observe a clear delay in the evolution of ammonia emissions in 2020 of -77 kt (**Figure 5c**),  
465 while only Scandinavian countries show positive changes. Hot-spots of negative evolution were seen  
466 in central Europe, mainly in the triptych of Northern Italy, Switzerland and Austria, for the reasons  
467 discussed in the previous paragraph. In Poland, [social](#) measures affected the daily lives of [citizens](#)  
468 [significantly](#) (Szczepańska and Pietrzyka, 2021) and might be the reason for the decreased evolution  
469 of ammonia emissions (**Figure 5c**). After the measures were relaxed, the evolution of the emissions  
470 rebounded slightly with respect to the reference period (2016 – 2019) as shown in **Figure 5d**. The  
471 changes in ammonia during the rebound period were concentrated in countries that were affected  
472 most severely from the lockdown restrictions, namely Northern Italy, Switzerland, Austria and  
473 Poland. The same has been reported [elsewhere](#) for several other pollutant emissions (Davis et al.,  
474 2022; Jackson et al., 2022).

Deleted: with important agricultural activity

Deleted: It is well-known that

Deleted: (Van Damme et al., 2022)

Deleted: corresponding to the two main fertilization periods (Paulot et al., 2014) and that atmospheric abundances are high throughout the entire spring–summer period due to agricultural activities and temperature dependent volatilization (Sutton et al., 2013)

Field Code Changed

Deleted: did not stop in spring

Deleted: ;

Deleted: the Ministry of Health enforced self-isolation measures and restrictions on civic freedoms, including access to public spaces, to contain the transmission of the disease. These

Deleted: significantly

Deleted: Polish

## 4 Discussion

### 4.1 Rising ammonia concentrations during the European lockdowns

One issue that has been overlooked is the concentrations of ammonia before, during and after the 2020 lockdowns in Europe. Despite the delay in the emissions during the lockdown period in 2020 (section 3.4), satellite ammonia from CrIS showed an increase during the lockdowns and declined after the restrictions were relaxed in almost all European countries (Figure 4). The latter was reported in several studies analysing ground-based measurements. For example, Lovarelli et al. (2021) concluded that contrary to other air pollutants, ammonia was not reduced when the COVID-19 restrictions were introduced in North Italy. They further reported that urban and rural ammonia was the highest compared to previous years during the same months for which the strictest lockdowns occurred (i.e., spring 2020). Rennie et al. (2020) reported a slight decrease of ammonia in the UK, while Xu et al. (2022) observed increased of ambient ammonia during the lockdowns in China. Accordingly, Viatte et al. (2021) found enhanced ammonia during lockdown in Paris. Finally, in a recent study, Kuttippurath et al. (2023) reported increase in ammonia during lockdowns almost everywhere, with maxima in Western Europe, Eastern China, the Indian subcontinent and the Eastern USA. Since atmospheric ammonia has been increasing globally due to various anthropogenic activities, the European lockdowns in 2020 offer a unique opportunity to expose ammonia's sources and address the importance of secondary PM<sub>2.5</sub> formation.

Figure 6a depicts the modelled atmospheric lifetime of ammonia and its dependence from the calculated loss-rates over Europe for the first half of 2020. Ammonia is a particularly interesting substance due to its affinity to react with atmospheric sulfuric and nitric acids producing secondary aerosols. However, the reaction with sulfuric acid is more prevalent due to several factors. For instance, sulfuric acid is a stronger acid than nitric acid, leading to more efficient reactions with ammonia (higher reaction rate constant for ammonia with sulfuric than with nitric acid, thus faster formation of ammonium sulfate) (Behera and Sharma, 2012). Furthermore, ammonium sulfate (final product of ammonia reaction with sulfuric acid) is less volatile and more thermodynamically stable than ammonium nitrate (product of the reaction with nitric acid) favoring the formation and persistence of ammonium sulfate particles in the atmosphere (Walters et al., 2019). Finally, sulfuric acid forms more stable clusters with ammonia, even in the presence of nitric acid (Liu et al., 2018). Results from laboratory and field studies have confirmed that ammonia actually promotes the nucleation of sulfuric acid in the atmosphere (Weber et al., 1999; Schobesberger et al., 2015). The CLOUD (Cosmics Leaving Outdoor Droplets) experiment has also highlighted that ammonia preferentially reacts with sulfuric acid in the atmosphere due to its strong acidity, ability to drive

**Deleted:** <#>Uncertainty of the posterior emissions

As described in section 2.3 in more detail, we considered 4° surroundings of each spatial element of our inversion domain from which the CrIS observations were used in the inverse problem. This means that 45 spatial elements in CrIS space were used, with six vertical levels each, for each of the 26 temporal emission elements. To calculate the associated uncertainty of the posterior estimates, we tested two sources of uncertainty: (i) how different surroundings for each spatial element affect posterior emissions of ammonia and (ii) how the use of different prior emissions affects posterior ammonia. We organized a series of sensitivity tests using surroundings covering 2°, 3° and 4° from each grid-cell. This selection is realistic as it was shown previously in Cao et al. (2020) for the construction of prior emission error covariance matrix. For the second source of uncertainty, we performed the same inversion using not only EC6G4 and VD priors, but also adding results using two more datasets for ammonia (in total four), which have 10 times higher emissions, namely EGG and NE (see section 2.3).

The calculated absolute uncertainties are depicted in Figure 5a–c together with the relative uncertainty (Figure 5d) with respect to the posterior emissions of ammonia (posterior ammonia is shown in Figure 2c). The first source of uncertainty (different surroundings) slightly affects the resulting posterior emissions of ammonia (Figure 5a) causing an average relative uncertainty below 4% in the European emissions. The second source of uncertainty (use of different priors) causes much larger bias as shown in Figure 5b (average relative uncertainty 35%). The reason for this is obviously the large variation of the EGG (Bouwman et al., 1997; Giglio et al., 2013; Klimont et al., 2017) and NE (Evangelou et al., 2021) prior datasets that have total emissions in the first half of 2020 of 63.5 and 53.3 Tg, respectively, in contrast to only 6.2 and 5.7 Tg for EC6G4 and VD. Hence, the results presented here are sensitive to the use of prior emission dataset. The modelled concentrations (that replaces the hypothetical true column concentration in Eq. 1) is calculated by the SRMs and the prior emission and, therefore, play a key role in the comparison of the CrIS value ( $v^{sat}$ ) and retrieved value ( $v^{ret}$ ) (see Eq. 2). Also, the modelled concentrations stand as the argument of the natural logarithm weighted by the averaging kernel in logarithmic space. The linearization of this operator as suggested by Sitwell and Shephard (2021) may reduce the dependency on the prior emission term, however, this is beyond the scope of this study. Over (... [1])

**Deleted:** the

**Deleted:** measured atmospheric levels of

**Deleted:** recorded in

**Deleted:** , as agricultural activity, which is the main emissive source of this pollutant, was not interrupted

**Deleted:** took place

**Deleted:** s

**Deleted:** acids

**Deleted:** s

**Deleted:** In most cases, it is depleted by sulfuric and nitric acids. In principle, the neutralisation of sulfuric acid is faster and sulfuric acid more abundant in the atmosphere than nitric acid (Evangelou et al., 2021), so that ammonia is deple (... [2])

**Deleted:** (Weber et al., 1999; Schobesberger et al., 2015) suggest ...

**Formatted:** Font: Not Bold

646 [stable aerosol formation, and significant nucleation enhancement effects \(Kirkby et al., 2016; Wang](#)  
647 [et al., 2022\).](#) [Nitric acid plays a secondary role, primarily forming ammonium nitrate once sulfuric](#)  
648 [acid has reacted, but its contribution is limited by its volatility.](#)

649 During the lockdown period over Europe, transport and industrial activities mostly stopped,  
650 and consequently the related emissions also decreased. This had an immediate effect on  $SO_2$  and  $NO_x$   
651 (Guevara et al., 2021; Doumbia et al., 2021). Reductions of  $SO_2$  and  $NO_x$  caused less production of  
652 atmospheric sulfuric and nitric acids. The latter had a rapid twofold effect on the lifetime of ammonia:  
653 (i) Less available atmospheric acids needed less ammonia for [reaction](#) towards sulfate (mainly) and  
654 nitrate aerosols ([secondarily](#)) and therefore the loss-rates declined (**Figure 6a**) leading to  
655 accumulation of ammonia in its free form; (ii) ammonia originates mainly from agriculture and  
656 livestock, and these activities [were slightly affected](#) during the European lockdowns increasing the  
657 associated emissions (see **Figure 2**, though with a lower trend than previous years as discussed in  
658 section 3.4). The rising levels of ammonia during the COVID-19 lockdowns in Europe have been  
659 confirmed by the CrIS observations (**Figure 2** and **3**) and have been also reported elsewhere  
660 (Kuttippurath et al., 2023; Viatte et al., 2021; Xu et al., 2022; Lovarelli et al., 2021).

#### 661 4.2 Disturbance in the secondary formation of PM<sub>2.5</sub>

662 The response of the restriction measures on PM<sub>2.5</sub> mass concentrations suggests a  
663 relationship that is more complex than expected and beyond road traffic intensity, at least for Europe.  
664 It has been reported that there was no systematic decrease in PM<sub>2.5</sub> concentrations during COVID-  
665 19 lockdowns in [the USA](#) (Archer et al., 2020; Bekbulat et al., 2021) or even in Chinese cities (Mo  
666 et al., 2021), where primary sources are abundant and stringent lockdown measures decreased PM  
667 levels (Zhang et al., 2023). In a recent study focusing on PM<sub>2.5</sub> measurements over 30 urban and  
668 regional background European sites, Putaud et al. (2023) showed that the implementation of the  
669 lockdown measures resulted in minor increases in PM<sub>2.5</sub> mass concentration in Europe of  $+5\pm 33\%$ .  
670 The latter aligns well with several regional studies focusing on the impact of lockdowns to regional  
671 pollution (Querol et al., 2021; Shi et al., 2021; Viatte et al., 2021; Thunis et al., 2021; Putaud et al.,  
672 2021).

673 **Figure 6b** demonstrates observed PM<sub>2.5</sub> from the EMEP stations (78 sites) in comparison  
674 with modelled PM<sub>2.5</sub> concentrations, both averaged for all sites. In modelled PM<sub>2.5</sub> mass  
675 concentrations, we have separated primary and secondary PM<sub>2.5</sub>, as secondary PM<sub>2.5</sub> is modulated  
676 by the chemical state of the atmosphere as defined by the abundance in acids and free ammonia. We  
677 see that observed and modelled PM<sub>2.5</sub> concentrations are in good agreement in the first half of 2020.  
678 The good agreement between modelled and observed concentrations can be also confirmed for most  
679 of the EMEP stations over Europe with high Pearson's coefficients, low RMSE's and low standard  
680 deviations in the Taylor plot that is demonstrated in **Figure S 7**. Furthermore, while secondary PM<sub>2.5</sub>

**Deleted:** This effect is not well understood and results in rates of particle nucleation in the atmosphere that appear to be much faster than expected based on the theory.

**Deleted:** After the reaction with sulfuric acid, free ammonia can further react with nitric acid to form ammonium nitrate.

**Deleted:** However, in certain atmospheric conditions (e.g., high humidity, aqueous particles), the equilibrium vapor pressure of ammonia with nitric acid increases shifting the reaction with nitric acid towards production of free ammonia (Seinfeld and Pandis, 2000). However, production of ammonia is a rare event in continental Europe (see details in Tichý et al., 2023).

**Deleted:** neutralisation

**Deleted:** did not stop



695 constitute around 20-30% of the total PM2.5 (Dat et al., 2024; Bressi et al., 2013; Li et al., 2023), this  
696 proportion increased during the European lockdowns despite that reactions of ammonia to form  
697 PM2.5 were decelerated (as seen by the declined loss in **Figure 6a**).

698 Leung et al. (2020) reported that the abatement of nitrate in China is buffered not only by  
699 increased oxidant build-up, but also by **an increase in free ammonia concentrations** through sulfate  
700 concentration reduction, which favours **ammonium** nitrate formation. During COVID-19 restrictions  
701 in Europe, a significant decrease of  $NO_x$  (and  $SO_2$ ) emissions occurred (Guevara et al., 2021) also  
702 confirmed by Doumbia et al. (2021). Thunis et al. (2021) showed that the latter might have increased  
703 the oxidative capacity of the atmosphere and, in turn, PM2.5 formation. This is the main reason why  
704 PM2.5 concentrations were not decreased during the COVID-19 lockdowns in many European cities  
705 (Varotsos et al., 2021; Shi et al., 2021), while the same has been reported elsewhere (Huang et al.,  
706 2021; Le et al., 2020; Zhang et al., 2022).

707 PM2.5 increased at areas less affected by primary emissions during the 2020 lockdown, or at  
708 areas where the oxidative atmosphere favours secondary aerosol formation. For instance, reductions  
709 in PM2.5 were observed to be less pronounced than those in nitrogen dioxide in several regions (Patel  
710 et al., 2020; Shi and Brasseur, 2020), while PM2.5 even increased in others (Wang et al., 2020; Li et  
711 al., 2020). Li et al. (2020) indicated that while primary emissions dropped by 15–61% in China, daily  
712 average PM2.5 concentrations were still very high (15–79  $\mu\text{g m}^{-3}$ ) showing that background and  
713 residual pollutants were important. In a similar manner, an extreme PM2.5 pollution event during the  
714 Chinese lockdown in Nanning that cause public concern was due to secondary aerosol formation (Mo  
715 et al., 2021).

716 Here we aim at interpreting the mechanism below this disturbance in PM2.5 formation. As  
717 explained in Seinfeld and Pandis (2000) and represented in the LMDZ-INCA model (Hauglustaine  
718 et al., 2014), the neutralisation of atmospheric acids by ammonia in the atmosphere occurs **through**  
719 ammonium sulfate **formation**. Sulfate ( $SO_4^{2-}$ ) **is also** produced from sulfur dioxide ( $SO_2$ ) **gas**  
720 **phase oxidation by the** hydroxyl radical ( $OH$ ). Note that **the** hydroxyl radical is **mostly** formed in the  
721 atmosphere when ultraviolet **radiation** (UV) **photolyzes** ozone in the presence of water vapour, hence  
722 it is linked to humidity (**Figure S 8**). Sulfate production can also occur in the aqueous phase (Hoyle  
723 et al., 2016) through sulfur dioxide ( $SO_2$ ) oxidation with ozone ( $O_3$ ) or hydrogen peroxide  
724 ( $H_2O_2$ ). In both phases, **a** higher humidity favors sulfate formation (**Figure S 8**). Ammonia also  
725 reacts with nitric acid ( $HNO_3$ ) to form **ammonium** nitrate ( $NO_3^-$ ) in an equilibrium reaction. In  
726 that case, as  $SO_2$  is strongly decreased due to the restrictions (Doumbia et al., 2021) and more free  
727 ammonia accumulates (see previous section), these higher gaseous ammonia levels **increase the**  
728 **particulate nitrate formation**. This mechanism has been highlighted in China as an unintended

Deleted: sulfate to nitrate conversion and liberation of

Deleted: s

Deleted: (Hauglustaine et al., 2014)

Deleted: directly

Deleted:

Deleted: to

Deleted:

Deleted: () in the gas phase or to ammonium () and sulfate () with an intermediate product (ammonium, , and bisulfate, ) in the aqueous phase

Deleted: can

Deleted:

Deleted: be

Deleted: also

Deleted:

Deleted:

Deleted: in the gas phase

Deleted: with

Deleted: as the oxidant

Deleted: light

Deleted: from the sun strikes

Deleted: u

Deleted: ùù

Deleted: that is rare

Deleted: shift the equilibrium reaction towards

Deleted: a larger

Deleted: conversion of gaseous nitric acid into

Deleted:

757 consequence of the of  $NO_x$  and  $SO_2$  regulation on the PM2.5 levels (Lachatre et al., 2019).  
 758 Conducting specific experiment in the frame of the CLOUD collaboration, Wang et al. (2022)  
 759 reported that the  $NH_3$  -  $H_2SO_4$  -  $HNO_3$  system forms particles synergistically, at rates orders of  
 760 magnitude faster than those the individual reactions of ammonia with sulfuric or nitric acid can give.  
 761 In addition to this mechanism, as the fraction of the total inorganic nitrate, as particulate  $NO_3^-_{(s)}$   
 762 (instead of gaseous  $HNO_3_{(g)}$ ), increases, and as  $NO_x$  and  $SO_2$  decrease, while  $NH_3$  emissions remain  
 763 high, a small increase in the particulate fraction greatly slows down deposition of total inorganic  
 764  $NO_3^-_{(s)}$  and hence drives particulate  $NO_3^-_{(s)}$  to increase (Zhai et al., 2021). Thus, although  $NO_x$   
 765 emissions decreased during COVID-19 lockdowns in Europe, secondary PM2.5 stayed unchanged,  
 766 because  $NO_x$  emissions reduction drives faster oxidation of  $NO_x$  and slower deposition of total  
 767 inorganic  $NO_3^-_{(s)}$ .

Deleted: recently

Deleted: from any two of the three components

Deleted: and that the reaction rates are controlled by the availability of  $NH_3$ .

Deleted: emissions of

Deleted: the

## 768 5 Conclusion

769 We have examined the impact of lockdown measures in Europe due to COVID-19 on the  
 770 atmospheric levels and emissions of ammonia using high-resolution satellite observations combined  
 771 with a dispersion model and an inverse modelling algorithm. We find that ammonia emissions in  
 772 2020 declined by -9.8% as compared to the same period in previous years (2016–2019). However,  
 773 this decrease is insensitive to the meteorological conditions, as the 2020 ammonia emissions during  
 774 the European lockdowns dropped outside of the deviation of the emissions in the reference period  
 775 (2016–2019), while temperature, humidity and precipitation showed limited variability.

Deleted: appears to be

Deleted: in the 2020

Deleted: under the variance of emissions calculated for the reference period

Deleted: A

Deleted: because of agriculture and temperature dependent volatilization

Deleted: .

Deleted: Though

Deleted: of 2020

Deleted: ammonia

Deleted: found

Deleted: over Europe

Deleted: decreased

776 While ammonia emissions generally increase in spring and late summer in Europe due to  
 777 fertilisation, during the 2020 lockdowns, a clear delay in the evolution of the emissions of -77 kt was  
 778 calculated, mostly in the central European countries, which suffered by the stringent restrictions. The  
 779 evolution of ammonia emissions slightly rebounded after the restrictions were relaxed.

780 During the COVID-19 lockdowns of 2020 over Europe the atmospheric levels of ammonia  
 781 were drastically increased, as confirmed by ground-based and satellite observations. The reason for  
 782 this is twofold; first, the European lockdown measures reduced atmospheric emissions and levels of  
 783  $SO_2$  and  $NO_x$  and their acidic products ( $H_2SO_4$  and  $HNO_3$ ) slowing down binding and chemical  
 784 removal of ammonia (lifetimes increased), and thus accumulating free ammonia; second, the prevail  
 785 of agricultural activity during the lockdowns increased ammonia emissions, (though at a lower rate).

Deleted: never ceased constantly

Deleted: ing

Deleted: during the lockdowns,

Deleted: increase

786 Surprisingly, despite all the travel, working and social restrictions that the European  
 787 governments took to combat the outbreak of COVID-19, ambient pollution levels did not change as  
 788 expected. PM2.5 levels were modulated by the chemical state of the atmosphere through secondary

813 aerosol formation. Secondary PM<sub>2.5</sub> rather increased during the European lockdowns despite that the  
814 precursors of H<sub>2</sub>SO<sub>4</sub> and HNO<sub>3</sub> declined. More sulfate was produced from SO<sub>2</sub> and OH (gas phase)  
815 or O<sub>3</sub> (aqueous phase), while both atmospheric reactions were favoured by higher water vapour  
816 (humidity) during the lockdown period. The accumulated ammonia reacted with H<sub>2</sub>SO<sub>4</sub> first  
817 producing sulfate. Then, as SO<sub>2</sub> decreased during the European lockdowns and more free ammonia  
818 accumulated, the high excess gaseous ammonia reacted with HNO<sub>3</sub> shifting the equilibrium reaction  
819 towards conversion to particulate nitrate causing unintended increase in the PM<sub>2.5</sub> levels. While NO<sub>x</sub>  
820 emissions declined during the European lockdowns by -33%, this reduction drives faster oxidation of  
821 NO<sub>x</sub> and slower deposition of total inorganic nitrate causing high secondary PM<sub>2.5</sub> levels.

822 The present study gives a comprehensive analysis of the atmospheric NH<sub>3</sub> - H<sub>2</sub>SO<sub>4</sub> - HNO<sub>3</sub>  
823 system. It also proves the complicated relationship of secondary PM<sub>2.5</sub> formation with the abundant  
824 atmospheric gases. The general drop of emissions during the first consistent lockdowns of 2020 in  
825 Europe offers a unique opportunity to study atmospheric chemistry under extreme conditions of fast  
826 pollutant emission drop equivalent to “The Clean Air Action” of the Chinese government.

827 **Data availability.** All data from this study are available for download from  
828 <https://datadryad.org/stash/share/Wgbc9UiXwtMH44366myWh2bt7MQc92JKhJBz7UwQlgY>  
829 (reserved doi: 10.5061/dryad.12jm63z1q). The EMEP measurements of ammonia can be downloaded  
830 from <https://ebas.nilu.no>. The remote sensing data for ammonia can be retrieved from  
831 [https://hpfx.collab.science.gc.ca/~mas001/satellite\\_ext/cris/snpp/nh3/v1\\_6\\_4/](https://hpfx.collab.science.gc.ca/~mas001/satellite_ext/cris/snpp/nh3/v1_6_4/) or upon request to Dr.  
832 M. W. Shephard. FLEXPART version 10.4 model can be downloaded from  
833 <https://www.flexpart.eu/downloads>.  
834

835 **Supplement.** The supplement related to this article is available online at.  
836

837 **Author contributions.** NE led the overall study, analysed the results and wrote the paper. OT  
838 developed the inverse modelling algorithm and performed the inversions. MSO processed CrIS  
839 ammonia on a grid. SE developed FLEXPART version 10.4 model to account for the loss of ammonia  
840 from the chemistry transport model LMDz-OR-INCA. YB and DH set up and ran the chemistry  
841 transport model LMDz-OR-INCA. All authors contributed to the final version of the manuscript.  
842

843 **Competing interests.** The authors declare no competing interests.  
844  
845

Deleted: content

Deleted: neutralised

Deleted: the more abundant

Deleted: neutralised

Deleted: system

Deleted: s

Deleted: their

853 **Financial support.** The work was supported by the COMBAT (Quantification of Global Ammonia  
854 Sources constrained by a Bayesian Inversion Technique) project funded by ROMFORSK – Program  
855 for romforskning of the Research Council of Norway (Project ID: 275407, website:  
856 [https://prosjektbanken.forskingsradet.no/project/FORISS/275407?Kilde=FORISS&distribution=Ar](https://prosjektbanken.forskingsradet.no/project/FORISS/275407?Kilde=FORISS&distribution=Ar&chart=bar&calcType=funding&Sprak=no&sortBy=date&sortOrder=desc&resultCount=30&offset=0&ProgAkt.3=ROMFORSK-Program+for+romforskning)  
857 [r&chart=bar&calcType=funding&Sprak=no&sortBy=date&sortOrder=desc&resultCount=30&offse](https://prosjektbanken.forskingsradet.no/project/FORISS/275407?Kilde=FORISS&distribution=Ar&chart=bar&calcType=funding&Sprak=no&sortBy=date&sortOrder=desc&resultCount=30&offset=0&ProgAkt.3=ROMFORSK-Program+for+romforskning)  
858 [t=0&ProgAkt.3=ROMFORSK-Program+for+romforskning](https://prosjektbanken.forskingsradet.no/project/FORISS/275407?Kilde=FORISS&distribution=Ar&chart=bar&calcType=funding&Sprak=no&sortBy=date&sortOrder=desc&resultCount=30&offset=0&ProgAkt.3=ROMFORSK-Program+for+romforskning)). Dr. Ondřej Tichý was supported by the  
859 Czech Science Foundation, grant no. [GA24-10400S](#).

Deleted: GA20-27939S

## 861 References

862 [Abbatt, J. P. D., Benz, S., Cziczo, D. J., Kanji, Z., Lohmann, U., and Mohler, O.: Solid Ammonium](#)  
863 [Sulfate Aerosols as Ice Nuclei: A Pathway for Cirrus Cloud Formation, \*Science\* \(80-. \), 313, 1770–](#)  
864 [1773, 2006.](#)

865 [Acharya, P., Barik, G., Gayen, B. K., Bar, S., Maiti, A., Sarkar, A., Ghosh, S., De, S. K., and](#)  
866 [Sreelesh, S.: Revisiting the levels of Aerosol Optical Depth in south-southeast Asia, Europe and](#)  
867 [USA amid the COVID-19 pandemic using satellite observations, \*Environ. Res.\*, 193, 110514,](#)  
868 <https://doi.org/10.1016/j.envres.2020.110514>, 2021.

869 [Anderson, N., Strader, R., and Davidson, C.: Airborne reduced nitrogen: Ammonia emissions from](#)  
870 [agriculture and other sources, \*Environ. Int.\*, 29, 277–286, \[https://doi.org/10.1016/S0160-\]\(https://doi.org/10.1016/S0160-4120\(02\)00186-1\)](#)  
871 [4120\(02\)00186-1](https://doi.org/10.1016/S0160-4120(02)00186-1), 2003.

872 [Archer, C. L., Cervone, G., Golbazi, M., Al Fahel, N., and Hultquist, C.: Changes in air quality and](#)  
873 [human mobility in the USA during the COVID-19 pandemic, \*Bull. Atmos. Sci. Technol.\*, 1, 491–](#)  
874 [514, <https://doi.org/10.1007/s42865-020-00019-0>, 2020.](https://doi.org/10.1007/s42865-020-00019-0)

875 [Baekgaard, M., Christensen, J., Madsen, J. K., and Mikkelsen, K. S.: Rallying around the flag in](#)  
876 [times of COVID-19: Societal lockdown and trust in democratic institutions, \*J. Behav. Public Adm.\*,](#)  
877 [3, 1–12, <https://doi.org/10.30636/jbpa.32.172>, 2020.](https://doi.org/10.30636/jbpa.32.172)

878 [Bauwens, M., Compennolle, S., Stavrakou, T., Müller, J. F., van Gent, J., Eskes, H., Levelt, P. F.,](#)  
879 [van der A, R., Veefkind, J. P., Vlietinck, J., Yu, H., and Zehner, C.: Impact of Coronavirus](#)  
880 [Outbreak on NO2 Pollution Assessed Using TROPOMI and OMI Observations, \*Geophys. Res.\*](#)  
881 [Lett.](#), 47, 1–9, <https://doi.org/10.1029/2020GL087978>, 2020.

882 [Behera, S. N. and Sharma, M.: Transformation of atmospheric ammonia and acid gases into](#)  
883 [components of PM2.5: An environmental chamber study, \*Environ. Sci. Pollut. Res.\*, 19, 1187–1197,](#)  
884 <https://doi.org/10.1007/s11356-011-0635-9>, 2012.

885 [Bekbulat, B., Apte, J. S., Millet, D. B., Robinson, A. L., Wells, K. C., Presto, A. A., and Marshall,](#)  
886 [J. D.: Changes in criteria air pollution levels in the US before, during, and after Covid-19 stay-at-](#)  
887 [home orders: Evidence from regulatory monitors, \*Sci. Total Environ.\*, 769, 144693,](#)

Formatted: Font: 12 pt

Formatted: Space After: 0 pt, Line spacing: 1.5 lines

889 <https://doi.org/10.1016/j.scitotenv.2020.144693>, 2021.

890 [Bellouin, N., Rae, J., Jones, A., Johnson, C., Haywood, J., and Boucher, O.: Aerosol forcing in the](#)  
891 [Climate Model Intercomparison Project \(CMIP5\) simulations by HadGEM2-ES and the role of](#)  
892 [ammonium nitrate, \*J. Geophys. Res. Atmos.\*, 116, 1–25, <https://doi.org/10.1029/2011JD016074>,](#)  
893 [2011.](#)

894 [Bendz, B. and Aaberge, L.: COVID-19 spread in the UK: the end of the beginning?, \*Lancet\*, 396,](#)  
895 [587–590, \[https://doi.org/https://doi.org/10.1016/S0140-6736\\(20\\)31689-5\]\(https://doi.org/https://doi.org/10.1016/S0140-6736\(20\)31689-5\) \[www.thelancet.com\]\(http://www.thelancet.com\),](#)  
896 [2020.](#)

897 [Bouwman, A. F., Lee, D. S., Asman, W. A. H., Dentener, F. J., Van Der Hoek, K. W., and Olivier,](#)  
898 [J. G. J.: A global high-resolution emission inventory for ammonia, \*Global Biogeochem. Cycles\*, 11,](#)  
899 [561–587, <https://doi.org/10.1029/97GB02266>, 1997.](#)

900 [Bressi, M., Sciare, J., Ghersi, V., Bonnaire, N., Nicolas, J. B., Petit, J. E., Moukhtar, S., Rosso, A.,](#)  
901 [Mihalopoulos, N., and Féron, A.: A one-year comprehensive chemical characterisation of fine](#)  
902 [aerosol \(PM<sub>2.5</sub>\) at urban, suburban and rural background sites in the region of Paris \(France\),](#)  
903 [Atmos. Chem. Phys., 13, 7825–7844, <https://doi.org/10.5194/acp-13-7825-2013>, 2013.](#)

904 [Camargo, J. A. and Alonso, Á.: Ecological and toxicological effects of inorganic nitrogen pollution](#)  
905 [in aquatic ecosystems: A global assessment, \*Environ. Int.\*, 32, 831–849,](#)  
906 [https://doi.org/10.1016/j.envint.2006.05.002, 2006.](#)

907 [Cao, H., Henze, D. K., Shephard, M. W., Dammers, E., Cady-Pereira, K., Alvarado, M., Lonsdale,](#)  
908 [C., Luo, G., Yu, F., Zhu, L., Danielson, C. G., and Edgerton, E. S.: Inverse modeling of NH<sub>3</sub>](#)  
909 [sources using CrIS remote sensing measurements, \*Environ. Res. Lett.\*, 15, 104082,](#)  
910 [https://doi.org/10.1088/1748-9326/abb5cc, 2020.](#)

911 [Cassiani, M., Stohl, A., and Brioude, J.: Lagrangian Stochastic Modelling of Dispersion in the](#)  
912 [Convective Boundary Layer with Skewed Turbulence Conditions and a Vertical Density Gradient:](#)  
913 [Formulation and Implementation in the FLEXPART Model, \*Boundary-Layer Meteorol.\*, 154, 367–](#)  
914 [390, <https://doi.org/10.1007/s10546-014-9976-5>, 2015.](#)

915 [Chakraborty, I. and Maity, P.: COVID-19 outbreak: Migration, effects on society, global](#)  
916 [environment and prevention, \*Sci. Total Environ.\*, 728, 138882,](#)  
917 [https://doi.org/10.1016/j.scitotenv.2020.138882, 2020.](#)

918 [Chen, S., Perathoner, S., Ampelli, C., and Centi, G.: Chapter 2 - Electrochemical Dinitrogen](#)  
919 [Activation: To Find a Sustainable Way to Produce Ammonia, in: \*Horizons in Sustainable Industrial\*](#)  
920 [Chemistry and Catalysis, vol. 178, edited by: Albonetti, S., Perathoner, S., and Quadrelli, E. A. B.](#)  
921 [T.-S. in S. S. and C., Elsevier, 31–46, \[https://doi.org/https://doi.org/10.1016/B978-0-444-64127-\]\(https://doi.org/https://doi.org/10.1016/B978-0-444-64127-4.00002-1\)](#)  
922 [4.00002-1, 2019.](#)

923 [Cohen, A. J., Brauer, M., Burnett, R., Anderson, H. R., Frostad, J., Estep, K., Balakrishnan, K.,](#)

924 [Brunekreef, B., Dandona, L., Dandona, R., Feigin, V., Freedman, G., Hubbell, B., Jobling, A., Kan,](#)  
925 [H., Knibbs, L., Liu, Y., Martin, R., Morawska, L., Pope, C. A., Shin, H., Straif, K., Shaddick, G.,](#)  
926 [Thomas, M., van Dingenen, R., van Donkelaar, A., Vos, T., Murray, C. J. L., and Forouzanfar, M.](#)  
927 [H.: Estimates and 25-year trends of the global burden of disease attributable to ambient air](#)  
928 [pollution: an analysis of data from the Global Burden of Diseases Study 2015, \*Lancet\*, 389, 1907–](#)  
929 [1918, \[https://doi.org/10.1016/S0140-6736\\(17\\)30505-6\]\(https://doi.org/10.1016/S0140-6736\(17\)30505-6\), 2017.](#)  
930 [Croft, B., Pierce, J. R., and Martin, R. V.: Interpreting aerosol lifetimes using the GEOS-Chem](#)  
931 [model and constraints from radionuclide measurements, \*Atmos. Chem. Phys.\*, 14, 4313–4325,](#)  
932 [<https://doi.org/10.5194/acp-14-4313-2014>, 2014.](#)  
933 [Van Damme, M., Clarisse, L., Whitburn, S., Hadji-Lazaro, J., Hurtmans, D., Clerbaux, C., and](#)  
934 [Coheur, P. F.: Industrial and agricultural ammonia point sources exposed, \*Nature\*, 564, 99–103,](#)  
935 [<https://doi.org/10.1038/s41586-018-0747-1>, 2018.](#)  
936 [Van Damme, M., Clarisse, L., Franco, B., Sutton, M. A., Erisman, J. W., Wichink Kruit, R., Van](#)  
937 [Zanten, M., Whitburn, S., Hadji-Lazaro, J., Hurtmans, D., Clerbaux, C., and Coheur, P. F. ois:](#)  
938 [Global, regional and national trends of atmospheric ammonia derived from a decadal \(2008–2018\)](#)  
939 [satellite record, \*Environ. Res. Lett.\*, 16, <https://doi.org/10.1088/1748-9326/abd5e0>, 2021.](#)  
940 [Van Damme, M., Clarisse, L., Stavrou, T., Wichink Kruit, R., Sellekaerts, L., Viatte, C.,](#)  
941 [Clerbaux, C., and Coheur, P. F.: On the weekly cycle of atmospheric ammonia over European](#)  
942 [agricultural hotspots, \*Sci. Rep.\*, 12, 1–9, <https://doi.org/10.1038/s41598-022-15836-w>, 2022.](#)  
943 [Dammers, E., Shephard, M. W., Palm, M., Cady-pereira, K., Capps, S., Lutsch, E., Strong, K.,](#)  
944 [Hannigan, J. W., Ortega, I., Toon, G. C., Stremme, W., and Grutter, M.: Validation of the CrIS fast](#)  
945 [physical NH<sub>3</sub> retrieval with ground-based FTIR, \*Atmos. Meas. Tech.\*, 87, 2645–2667, 2017.](#)  
946 [Dat, N. Q., Ly, B. T., Nghiem, T. D., Nguyen, T. T. H., Sekiguchi, K., Huyen, T. T., Vinh, T. H.,](#)  
947 [and Tien, L. Q.: Influence of Secondary Inorganic Aerosol on the Concentrations of PM<sub>2.5</sub> and](#)  
948 [PM<sub>0.1</sub> during Air Pollution Episodes in Hanoi, Vietnam, \*Aerosol Air Qual. Res.\*, 24,](#)  
949 [<https://doi.org/10.4209/aaqr.220446>, 2024.](#)  
950 [Davis, S. J., Liu, Z., Deng, Z., Zhu, B., Ke, P., Sun, T., Guo, R., Hong, C., Zheng, B., Wang, Y.,](#)  
951 [Boucher, O., Gentine, P., and Ciais, P.: Emissions rebound from the COVID-19 pandemic, \*Nat.\*](#)  
952 [\*Clim. Chang.\*, 12, 410–417, <https://doi.org/10.1038/s41558-022-01351-3>, 2022.](#)  
953 [Diffenbaugh, N. S., Field, C. B., Appel, E. A., Azevedo, I. L., Baldocchi, D. D., Burke, M., Burney,](#)  
954 [J. A., Ciais, P., Davis, S. J., Fiore, A. M., Fletcher, S. M., Hertel, T. W., Horton, D. E., Hsiang, S.](#)  
955 [M., Jackson, R. B., Jin, X., Levi, M., Lobell, D. B., McKinley, G. A., Moore, F. C., Montgomery,](#)  
956 [A., Nadeau, K. C., Pataki, D. E., Randerson, J. T., Reichstein, M., Schnell, J. L., Seneviratne, S. I.,](#)  
957 [Singh, D., Steiner, A. L., and Wong-Parodi, G.: The COVID-19 lockdowns: a window into the](#)  
958 [Earth System, \*Nat. Rev. Earth Environ.\*, 1–12, <https://doi.org/10.1038/s43017-020-0079-1>, 2020.](#)

959 [Doumbia, T., Granier, C., Elguindi, N., Bouarar, I., Darras, S., Brasseur, G., Gaubert, B., Liu, Y.,](#)  
960 [Shi, X., Stavrakou, T., Tilmes, S., Lacey, F., Deroubaix, A., and Wang, T.: Changes in global air](#)  
961 [pollutant emissions during the COVID-19 pandemic: A dataset for atmospheric modeling, \*Earth\*](#)  
962 [Syst. Sci. Data, 13, 4191–4206, <https://doi.org/10.5194/essd-13-4191-2021>, 2021.](#)  
963 [Dutheil, F., Baker, J. S., and Navel, V.: COVID-19 as a factor influencing air pollution?, \*Environ.\*](#)  
964 [Pollut., 263, 2019–2021, <https://doi.org/10.1016/j.envpol.2020.114466>, 2020.](#)  
965 [Emanuel, K. A.: A Scheme for Representing Cumulus Convection in Large-Scale Models, \*J.\*](#)  
966 [Atmos. Sci., 48, 2313–2329, \[https://doi.org/10.1175/1520-\]\(https://doi.org/10.1175/1520-0469\(1991\)048<2313:ASFRCC>2.0.CO;2\)](#)  
967 [0469\(1991\)048<2313:ASFRCC>2.0.CO;2, 1991.](#)  
968 [Erisman, J. W., Bleeker, A., Galloway, J., and Sutton, M. S.: Reduced nitrogen in ecology and the](#)  
969 [environment, \*Environ. Pollut.\*, 150, 140–149, <https://doi.org/10.1016/j.envpol.2007.06.033>, 2007.](#)  
970 [Erisman, J. W., Sutton, M. a., Galloway, J., Klimont, Z., and Winiwarer, W.: How a century of](#)  
971 [ammonia synthesis changed the world, \*Nat. Geosci.\*, 1, 636–639, <https://doi.org/10.1038/ngeo325>,](#)  
972 [2008.](#)  
973 [Evangelou, N., Platt, S., Eckhardt, S., Lund Myhre, C., Laj, P., Alados-Arboledas, L., Backman, J.,](#)  
974 [Brem, B., Fiebig, M., Flentje, H., Marinoni, A., Pandolfi, M., Yus-Diez, J., Prats, N., Putaud, J.,](#)  
975 [Sellegri, K., Sorribas, M., Eleftheriadis, K., Vratolis, S., Wiedensohler, A., and Stohl, A.: Changes](#)  
976 [in black carbon emissions over Europe due to COVID-19 lockdowns, \*Atmos. Chem. Phys.\*, 1–33,](#)  
977 [https://doi.org/10.5194/acp-2020-1005, 2020.](#)  
978 [Evangelou, N., Balkanski, Y., Eckhardt, S., Cozic, A., Van Damme, M., Coheur, P.-F., Clarisse,](#)  
979 [L., Shephard, M., Cady-Pereira, K., and Hauglustaine, D.: 10–Year Satellite–Constrained Fluxes of](#)  
980 [Ammonia Improve Performance of Chemistry Transport Models, \*Atmos. Chem. Phys.\*, 21, 4431–](#)  
981 [4451, <https://doi.org/10.5194/acp-21-4431-2021>, 2021.](#)  
982 [Folberth, G. A., Hauglustaine, D. A., Lathière, J., and Brocheton, F.: Interactive chemistry in the](#)  
983 [Laboratoire de Météorologie Dynamique general circulation model: model description and impact](#)  
984 [analysis of biogenic hydrocarbons on tropospheric chemistry, \*Atmos. Chem. Phys.\*, 6, 2273–2319,](#)  
985 [https://doi.org/10.5194/acp-6-2273-2006, 2006.](#)  
986 [Forster, C., Stohl, A., and Seibert, P.: Parameterization of convective transport in a Lagrangian](#)  
987 [particle dispersion model and its evaluation, \*J. Appl. Meteorol. Climatol.\*, 46, 403–422,](#)  
988 [https://doi.org/10.1175/JAM2470.1, 2007.](#)  
989 [Fowler, D., Muller, J. B. A., Smith, R. I., Dragosits, U., Skiba, U., Sutton, M. A., and](#)  
990 [Brimblecombe, P.: A CHRONOLOGY OF NITROGEN DEPOSITION IN THE UK, \*Water, Air,\*](#)  
991 [Soil Pollut. Focus, 4, 9–23, 2004.](#)  
992 [Ge, X., Schaap, M., Kranenburg, R., Segers, A., Jan Reinds, G., Kros, H., and De Vries, W.:](#)  
993 [Modeling atmospheric ammonia using agricultural emissions with improved spatial variability and](#)

994 [temporal dynamics, Atmos. Chem. Phys., 20, 16055–16087, https://doi.org/10.5194/acp-20-16055-](https://doi.org/10.5194/acp-20-16055-2020)  
995 [2020, 2020.](https://doi.org/10.5194/acp-20-16055-2020)

996 [Giani, P., Castruccio, S., Anav, A., Howard, D., Hu, W., and Crippa, P.: Short-term and long-term](https://doi.org/10.1016/S2542-5196(20)30224-2)  
997 [health impacts of air pollution reductions from COVID-19 lockdowns in China and Europe: a](https://doi.org/10.1016/S2542-5196(20)30224-2)  
998 [modelling study, Lancet Planet. Heal., 4, e474–e482, https://doi.org/10.1016/S2542-](https://doi.org/10.1016/S2542-5196(20)30224-2)  
999 [5196\(20\)30224-2, 2020.](https://doi.org/10.1016/S2542-5196(20)30224-2)

1000 [Giglio, L., Randerson, J. T., and van der Werf, G. R.: Analysis of daily, monthly, and annual burned](https://doi.org/10.1002/jgrg.20042)  
1001 [area using the fourth-generation global fire emissions database \(GFED4\), J. Geophys. Res.](https://doi.org/10.1002/jgrg.20042)  
1002 [Biogeosciences, 118, 317–328, https://doi.org/10.1002/jgrg.20042, 2013, 2013.](https://doi.org/10.1002/jgrg.20042)

1003 [Gordon, D. V., Grafton, R. Q., and Steinshamn, S. I.: Cross-country effects and policy responses to](https://doi.org/10.1016/j.eap.2021.04.015)  
1004 [COVID-19 in 2020: The Nordic countries, Econ. Anal. Policy, 71, 198–210,](https://doi.org/10.1016/j.eap.2021.04.015)  
1005 [https://doi.org/10.1016/j.eap.2021.04.015, 2021.](https://doi.org/10.1016/j.eap.2021.04.015)

1006 [Gu, B., Sutton, M. A., Chang, S. X., Ge, Y., and Chang, J.: Agricultural ammonia emissions](https://doi.org/10.1890/14.WB.007)  
1007 [contribute to China’s urban air pollution, Front. Ecol. Environ., 12, 265–266,](https://doi.org/10.1890/14.WB.007)  
1008 [https://doi.org/10.1890/14.WB.007, 2014.](https://doi.org/10.1890/14.WB.007)

1009 [Guevara, M., Jorba, O., Soret, A., Petetin, H., Bowdalo, D., Serradell, K., Tena, C., Van Der Gon,](https://doi.org/10.5194/acp-21-773-2021)  
1010 [H. D., Kuenen, J., Peuch, V. H., and Pérez García-Pando, C.: Time-resolved emission reductions for](https://doi.org/10.5194/acp-21-773-2021)  
1011 [atmospheric chemistry modelling in Europe during the COVID-19 lockdowns, Atmos. Chem.](https://doi.org/10.5194/acp-21-773-2021)  
1012 [Phys., 21, 773–797, https://doi.org/10.5194/acp-21-773-2021, 2021.](https://doi.org/10.5194/acp-21-773-2021)

1013 [Hauglustaine, D. A., Hourdin, F., Jourdain, L., Filiberti, M.-A., Walters, S., Lamarque, J.-F., and](https://doi.org/10.1029/2003JD003957)  
1014 [Holland, E. A.: Interactive chemistry in the Laboratoire de Meteorologie Dynamique general](https://doi.org/10.1029/2003JD003957)  
1015 [circulation model: Description and background tropospheric chemistry evaluation, J. Geophys.](https://doi.org/10.1029/2003JD003957)  
1016 [Res., 109, https://doi.org/10.1029/2003JD003957, 2004.](https://doi.org/10.1029/2003JD003957)

1017 [Hauglustaine, D. A., Balkanski, Y., and Schulz, M.: A global model simulation of present and](https://doi.org/10.5194/acp-14-11031-2014)  
1018 [future nitrate aerosols and their direct radiative forcing of climate, Atmos. Chem. Phys., 14, 11031–](https://doi.org/10.5194/acp-14-11031-2014)  
1019 [11063, https://doi.org/10.5194/acp-14-11031-2014, 2014.](https://doi.org/10.5194/acp-14-11031-2014)

1020 [Heald, C. L., Collett, J. L., Lee, T., Benedict, K. B., Schwandner, F. M., Li, Y., Clarisse, L.,](https://doi.org/10.5194/acp-12-10295-2012)  
1021 [Hurtmans, D. R., Van Damme, M., Clerbaux, C., Coheur, P. F., Philip, S., Martin, R. V., and Pye,](https://doi.org/10.5194/acp-12-10295-2012)  
1022 [H. O. T.: Atmospheric ammonia and particulate inorganic nitrogen over the United States, Atmos.](https://doi.org/10.5194/acp-12-10295-2012)  
1023 [Chem. Phys., 12, 10295–10312, https://doi.org/10.5194/acp-12-10295-2012, 2012.](https://doi.org/10.5194/acp-12-10295-2012)

1024 [Henze, D. K., Shindell, D. T., Akhtar, F., Spurr, R. J. D., Pinder, R. W., Loughlin, D., Kopacz, M.,](https://doi.org/10.1021/es301993s)  
1025 [Singh, K., and Shim, C.: Spatially Refined Aerosol Direct Radiative Forcing Efficiencies, Environ.](https://doi.org/10.1021/es301993s)  
1026 [Sci. Technol., 46, 9511–9518, https://doi.org/10.1021/es301993s, 2012.](https://doi.org/10.1021/es301993s)

1027 [Hersbach, H., Bell, B., Berrisford, P., Hirahara, S., Horányi, A., Muñoz-Sabater, J., Nicolas, J.,](https://doi.org/10.1016/j.atmosenv.2012.05.015)  
1028 [Peubey, C., Radu, R., Schepers, D., Simmons, A., Soci, C., Abdalla, S., Abellan, X., Balsamo, G.,](https://doi.org/10.1016/j.atmosenv.2012.05.015)



1029 [Bechtold, P., Biavati, G., Bidlot, J., Bonavita, M., De Chiara, G., Dahlgren, P., Dee, D.,](#)  
1030 [Diamantakis, M., Dragani, R., Flemming, J., Forbes, R., Fuentes, M., Geer, A., Haimberger, L.,](#)  
1031 [Healy, S., Hogan, R. J., Hólm, E., Janisková, M., Keeley, S., Laloyaux, P., Lopez, P., Lupu, C.,](#)  
1032 [Radnoti, G., de Rosnay, P., Rozum, I., Vamborg, F., Villaume, S., and Thépaut, J. N.: The ERA5](#)  
1033 [global reanalysis, Q. J. R. Meteorol. Soc., 146, 1999–2049, <https://doi.org/10.1002/qj.3803>, 2020.](#)  
1034 [Hourdin, F. and Armengaud, A.: The Use of Finite-Volume Methods for Atmospheric Advection of](#)  
1035 [Trace Species. Part I: Test of Various Formulations in a General Circulation Model, Mon. Weather](#)  
1036 [Rev., 127, 822–837, \[https://doi.org/10.1175/1520-0493\\(1999\\)127<0822:TUOFVM>2.0.CO;2\]\(https://doi.org/10.1175/1520-0493\(1999\)127<0822:TUOFVM>2.0.CO;2\),](#)  
1037 [1999.](#)  
1038 [Hourdin, F., Musat, I., Bony, S., Braconnot, P., Codron, F., Dufresne, J. L., Fairhead, L., Filiberti,](#)  
1039 [M. A., Friedlingstein, P., Grandpeix, J. Y., Krinner, G., LeVan, P., Li, Z. X., and Lott, F.: The](#)  
1040 [LMDZ4 general circulation model: Climate performance and sensitivity to parametrized physics](#)  
1041 [with emphasis on tropical convection, Clim. Dyn., 27, 787–813, \[https://doi.org/10.1007/s00382-\]\(https://doi.org/10.1007/s00382-006-0158-0\)](#)  
1042 [006-0158-0](#), 2006.  
1043 [Hoyle, C. R., Fuchs, C., Jarvinen, E., Saathoff, H., Dias, A., El Haddad, I., Gysel, M., Coburn, S.](#)  
1044 [C., Trostl, J., Hansel, A., Bianchi, F., Breitenlechner, M., Corbin, J. C., Craven, J., Donahue, N. M.,](#)  
1045 [Duplissy, J., Ehrhart, S., Frege, C., Gordon, H., Hoppel, N., Heinritzi, M., Kristensen, T. B.,](#)  
1046 [Molteni, U., Nichman, L., Pinterich, T., Prevôt, A. S. H., Simon, M., Slowik, J. G., Steiner, G.,](#)  
1047 [Tome, A., Vogel, A. L., Volkamer, R., Wagner, A. C., Wagner, R., Wexler, A. S., Williamson, C.,](#)  
1048 [Winkler, P. M., Yan, C., Amorim, A., Dommen, J., Curtius, J., Gallagher, M. W., Flagan, R. C.,](#)  
1049 [Hansel, A., Kirkby, J., Kulmala, M., Mohler, O., Stratmann, F., Worsnop, D. R., and Baltensperger,](#)  
1050 [U.: Aqueous phase oxidation of sulphur dioxide by ozone in cloud droplets, Atmos. Chem. Phys.,](#)  
1051 [16, 1693–1712, <https://doi.org/10.5194/acp-16-1693-2016>, 2016.](#)  
1052 [Huang, X., Ding, A., Gao, J., Zheng, B., Zhou, D., Qi, X., Tang, R., Wang, J., Ren, C., Nie, W.,](#)  
1053 [Chi, X., Xu, Z., Chen, L., Li, Y., Che, F., Pang, N., Wang, H., Tong, D., Qin, W., Cheng, W., Liu,](#)  
1054 [W., Fu, Q., Liu, B., Chai, F., Davis, S. J., Zhang, Q., and He, K.: Enhanced secondary pollution](#)  
1055 [offset reduction of primary emissions during COVID-19 lockdown in China, Natl. Sci. Rev., 8,](#)  
1056 [https://doi.org/10.1093/nsr/nwaa137, 2021.](#)  
1057 [Jackson, R. B., Friedlingstein, P., Quéré, C. Le, Abernethy, S., Andrew, R. M., Canadell, J. G.,](#)  
1058 [Ciais, P., Davis, S. J., Deng, Z., Liu, Z., Korsbakken, J. I., and Peters, G. P.: Global fossil carbon](#)  
1059 [emissions rebound near pre-COVID-19 levels, Environ. Res. Lett., 17,](#)  
1060 [https://doi.org/https://doi.org/10.1088/1748-9326/ac55b6, 2022.](#)  
1061 [Kean, A. J., Littlejohn, D., Ban-Weiss, G. A., Harley, R. A., Kirchstetter, T. W., and Lunden, M.](#)  
1062 [M.: Trends in on-road vehicle emissions of ammonia, Atmos. Environ., 43, 1565–1570,](#)  
1063 [https://doi.org/10.1016/j.atmosenv.2008.09.085, 2009.](#)

1064 [Kharol, S. K., Shephard, M. W., McLinden, C. A., Zhang, L., Sioris, C. E., O'Brien, J. M., Vet, R.,](#)  
1065 [Cady-Pereira, K. E., Hare, E., Siemons, J., and Krotkov, N. A.: Dry Deposition of Reactive](#)  
1066 [Nitrogen From Satellite Observations of Ammonia and Nitrogen Dioxide Over North America,](#)  
1067 [Geophys. Res. Lett., 45, 1157–1166, <https://doi.org/10.1002/2017GL075832>, 2018.](#)  
1068 [Kirkby, J., Duplissy, J., Sengupta, K., Frege, C., Gordon, H., Williamson, C., Heinritzi, M., Simon,](#)  
1069 [M., Yan, C., Almeida, J., Trostl, J., Nieminen, T., Ortega, I. K., Wagner, R., Adamov, A., Amorim,](#)  
1070 [A., Bernhammer, A. K., Bianchi, F., Breitenlechner, M., Brilke, S., Chen, X., Craven, J., Dias, A.,](#)  
1071 [Ehrhart, S., Flagan, R. C., Franchin, A., Fuchs, C., Guida, R., Hakala, J., Hoyle, C. R., Jokinen, T.,](#)  
1072 [Junninen, H., Kangasluoma, J., Kim, J., Krapf, M., Kurten, A., Laaksonen, A., Lehtipalo, K.,](#)  
1073 [Makhmutov, V., Mathot, S., Molteni, U., Onnela, A., Perakyla, O., Piel, F., Petaja, T., Praplan, A.](#)  
1074 [P., Pringle, K., Rap, A., Richards, N. A. D., Riipinen, I., Rissanen, M. P., Rondo, L., Sarnela, N.,](#)  
1075 [Schobesberger, S., Scott, C. E., Seinfeld, J. H., Sipila, M., Steiner, G., Stozhkov, Y., Stratmann, F.,](#)  
1076 [Tomé, A., Virtanen, A., Vogel, A. L., Wagner, A. C., Wagner, P. E., Weingartner, E., Wimmer, D.,](#)  
1077 [Winkler, P. M., Ye, P., Zhang, X., Hansel, A., Dommen, J., Donahue, N. M., Worsnop, D. R.,](#)  
1078 [Baltensperger, U., Kulmala, M., Carslaw, K. S., and Curtius, J.: Ion-induced nucleation of pure](#)  
1079 [biogenic particles, \*Nature\*, 533, 521–526, <https://doi.org/10.1038/nature17953>, 2016.](#)  
1080 [Klimont, Z.: personal communication, 2022.](#)  
1081 [Klimont, Z., Kupiainen, K., Heyes, C., Purohit, P., Cofala, J., Rafaj, P., Borken-Kleefeld, J., and](#)  
1082 [Schöpp, W.: Global anthropogenic emissions of particulate matter including black carbon, \*Atmos.\*](#)  
1083 [Chem. Phys., 17, 8681–8723, <https://doi.org/10.5194/acp-17-508681-2017>, 2017.](#)  
1084 [Krinner, G., Viovy, N., de Noblet-Ducoudré, N., Ogée, J., Polcher, J., Friedlingstein, P., Ciais, P.,](#)  
1085 [Sitch, S., and Prentice, I. C.: A dynamic global vegetation model for studies of the coupled](#)  
1086 [atmosphere-biosphere system, \*Global Biogeochem. Cycles\*, 19, GB1015,](#)  
1087 [https://doi.org/10.1029/2003GB002199, 2005.](#)  
1088 [Kristiansen, N. I., Stohl, A., Olivíe, D. J. L., Croft, B., Søvdé, O. A., Klein, H., Christoudias, T.,](#)  
1089 [Kunkel, D., Leadbetter, S. J., Lee, Y. H., Zhang, K., Tsigaridis, K., Bergman, T., Evangelidou, N.,](#)  
1090 [Wang, H., Ma, P. L., Easter, R. C., Rasch, P. J., Liu, X., Pitari, G., Di Genova, G., Zhao, S. Y.,](#)  
1091 [Balkanski, Y., Bauer, S. E., Faluvegi, G. S., Kokkola, H., Martin, R. V., Pierce, J. R., Schulz, M.,](#)  
1092 [Shindell, D., Tost, H., and Zhang, H.: Evaluation of observed and modelled aerosol lifetimes using](#)  
1093 [radioactive tracers of opportunity and an ensemble of 19 global models, 3525–3561 pp.,](#)  
1094 [https://doi.org/10.5194/acp-16-3525-2016, 2016.](#)  
1095 [Krupa, S. V.: Effects of atmospheric ammonia \(NH<sub>3</sub>\) on terrestrial vegetation: A review, \*Environ.\*](#)  
1096 [Pollut., 124, 179–221, \[https://doi.org/10.1016/S0269-7491\\(02\\)00434-7\]\(https://doi.org/10.1016/S0269-7491\(02\)00434-7\), 2003.](#)  
1097 [Kuttippurath, J., Patel, V. K., Kashyap, R., Singh, A., and Clerbaux, C.: Anomalous increase in](#)  
1098 [global atmospheric ammonia during COVID-19 lockdown: Need for policies to curb agricultural](#)

1099 [emissions, J. Clean. Prod., 434, 140424, https://doi.org/10.1016/j.jclepro.2023.140424, 2023.](https://doi.org/10.1016/j.jclepro.2023.140424)

1100 [Lachatre, M., Fortems-Cheiney, A., Foret, G., Siour, G., Dufour, G., Clarisse, L., Clerbaux, C.,](https://doi.org/10.5194/acp-19-6701-2019)

1101 [Coheur, P. F., Van Damme, M., and Beekmann, M.: The unintended consequence of SO<sub>2</sub> and NO<sub>2</sub>](https://doi.org/10.5194/acp-19-6701-2019)

1102 [regulations over China: Increase of ammonia levels and impact on PM<sub>2.5</sub> concentrations, Atmos.](https://doi.org/10.5194/acp-19-6701-2019)

1103 [Chem. Phys., 19, 6701–6716, https://doi.org/10.5194/acp-19-6701-2019, 2019.](https://doi.org/10.5194/acp-19-6701-2019)

1104 [Le, T., Wang, Y., Liu, L., Yang, J., Yung, Y. L., Li, G., and Seinfeld, J. H.: Unexpected air](https://doi.org/10.1126/science.abb7431)

1105 [pollution with marked emission reductions during the COVID-19 outbreak in China, Science \(80-](https://doi.org/10.1126/science.abb7431)

1106 [\), eabb7431, https://doi.org/10.1126/science.abb7431, 2020.](https://doi.org/10.1126/science.abb7431)

1107 [Lelieveld, J., Evans, J. S., Fnais, M., Giannadaki, D., and Pozzer, A.: The contribution of outdoor](https://doi.org/10.1038/nature15371)

1108 [air pollution sources to premature mortality on a global scale., Nature, 525, 367–71,](https://doi.org/10.1038/nature15371)

1109 [https://doi.org/10.1038/nature15371, 2015.](https://doi.org/10.1038/nature15371)

1110 [Leung, D. M., Shi, H., Zhao, B., Wang, J., Ding, E. M., Gu, Y., Zheng, H., Chen, G., Liou, K. N.,](https://doi.org/10.1029/2020GL087721)

1111 [Wang, S., Fast, J. D., Zheng, G., Jiang, J., Li, X., and Jiang, J. H.: Wintertime Particulate Matter](https://doi.org/10.1029/2020GL087721)

1112 [Decrease Buffered by Unfavorable Chemical Processes Despite Emissions Reductions in China,](https://doi.org/10.1029/2020GL087721)

1113 [Geophys. Res. Lett., 47, 1–12, https://doi.org/10.1029/2020GL087721, 2020.](https://doi.org/10.1029/2020GL087721)

1114 [Li, B., Ma, Y., Zhou, Y., and Chai, E.: Research progress of different components of PM<sub>2.5</sub> and](https://doi.org/10.1038/s41598-023-43119-5)

1115 [ischemic stroke, Sci. Rep., 13, 1–12, https://doi.org/10.1038/s41598-023-43119-5, 2023.](https://doi.org/10.1038/s41598-023-43119-5)

1116 [Li, C., Martin, R. V., Shephard, M. W., Pereira, K. C., Cooper, M. J., Kaiser, J., Lee, C. J., Zhang,](https://doi.org/10.1029/2018JD030183)

1117 [L., and Henze, D. K.: Assessing the Iterative Finite Difference Mass Balance and 4D - Var Methods](https://doi.org/10.1029/2018JD030183)

1118 [to Derive Ammonia Emissions Over North America Using Synthetic Observations, J. Geophys.](https://doi.org/10.1029/2018JD030183)

1119 [Res. Atmos., 124, 4222–4236, https://doi.org/10.1029/2018JD030183, 2019.](https://doi.org/10.1029/2018JD030183)

1120 [Li, L., Li, Q., Huang, L., Wang, Q., Zhu, A., Xu, J., Liu, Z., Li, H., Shi, L., Li, R., Azari, M., Wang,](https://doi.org/10.1016/j.scitotenv.2020.139282)

1121 [Y., Zhang, X., Liu, Z., Zhu, Y., Zhang, K., Xue, S., Ooi, M. C. G., Zhang, D., and Chan, A.: Air](https://doi.org/10.1016/j.scitotenv.2020.139282)

1122 [quality changes during the COVID-19 lockdown over the Yangtze River Delta Region: An insight](https://doi.org/10.1016/j.scitotenv.2020.139282)

1123 [into the impact of human activity pattern changes on air pollution variation, Sci. Total Environ.,](https://doi.org/10.1016/j.scitotenv.2020.139282)

1124 [732, https://doi.org/10.1016/j.scitotenv.2020.139282, 2020.](https://doi.org/10.1016/j.scitotenv.2020.139282)

1125 [Liu, L., Li, H., Zhang, H., Zhong, J., Bai, Y., Ge, M., Li, Z., Chen, Y., and Zhang, X.: The role of](https://doi.org/10.1039/C8CP02719F)

1126 [nitric acid in atmospheric new particle formation, Phys. Chem. Chem. Phys., 20, 17406–17414,](https://doi.org/10.1039/C8CP02719F)

1127 [https://doi.org/10.1039/C8CP02719F, 2018.](https://doi.org/10.1039/C8CP02719F)

1128 [Lovarelli, D., Fugazza, D., Costantini, M., Conti, C., Diolaiuti, G., and Guarino, M.: Comparison of](https://doi.org/10.1016/j.atmosenv.2021.118534)

1129 [ammonia air concentration before and during the spread of COVID-19 in Lombardy \(Italy\) using](https://doi.org/10.1016/j.atmosenv.2021.118534)

1130 [ground-based and satellite data, Atmos. Environ., 259, 118534,](https://doi.org/10.1016/j.atmosenv.2021.118534)

1131 [https://doi.org/10.1016/j.atmosenv.2021.118534, 2021.](https://doi.org/10.1016/j.atmosenv.2021.118534)

1132 [Malm, W. C.: Spatial and monthly trends in speciated fine particle concentration in the United](https://doi.org/10.1029/2003JD003739)

1133 [States, J. Geophys. Res., 109, D03306, https://doi.org/10.1029/2003JD003739, 2004.](https://doi.org/10.1029/2003JD003739)

1134 [Matthias, V., Quante, M., Arndt, J. A., Badeke, R., Fink, L., Petrik, R., Feldner, J., Schwarzkopf,](#)  
1135 [D., Link, E. M., Ramacher, M. O. P., and Wedemann, R.: The role of emission reductions and the](#)  
1136 [meteorological situation for air quality improvements during the COVID-19 lockdown period in](#)  
1137 [central Europe. \*Atmos. Chem. Phys.\*, 21, 13931–13971, \[https://doi.org/10.5194/acp-21-13931-\]\(https://doi.org/10.5194/acp-21-13931-2021\)](#)  
1138 [2021, 2021.](#)

1139 [Mo, Z., Huang, J., Chen, Z., Zhou, B., Zhu, K., Liu, H., Mu, Y., Zhang, D., and Wang, S.: Cause](#)  
1140 [analysis of PM<sub>2.5</sub> pollution during the COVID-19 lockdown in Nanning, China, \*Sci. Rep.\*, 11, 1–](#)  
1141 [13, <https://doi.org/10.1038/s41598-021-90617-5>, 2021.](#)

1142 [Pai, S. J., Heald, C. L., and Murphy, J. G.: Exploring the Global Importance of Atmospheric](#)  
1143 [Ammonia Oxidation, \*ACS Earth Sp. Chem.\*, 5, 1674–1685,](#)  
1144 [https://doi.org/10.1021/acsearthspacechem.1c00021, 2021.](#)

1145 [Patel, H., Talbot, N., Salmond, J., Dirks, K., Xie, S., and Davy, P.: Implications for air quality](#)  
1146 [management of changes in air quality during lockdown in Auckland \(New Zealand\) in response to](#)  
1147 [the 2020 SARS-CoV-2 epidemic, \*Sci. Total Environ.\*, 746, 141129,](#)  
1148 [https://doi.org/10.1016/j.scitotenv.2020.141129, 2020.](#)

1149 [Paulot, F., Jacob, D. J., Pinder, R. W., Bash, J. O., Travis, K., and Henze, D. K.: Ammonia](#)  
1150 [emissions in the United States, European Union, and China derived by high-resolution inversion of](#)  
1151 [ammonium wet deposition data: Interpretation with a new agricultural emissions inventory](#)  
1152 [\(MASAGE-NH<sub>3</sub>\), \*J. Geophys. Res. Atmos.\*, 119, 4343–4364,](#)  
1153 [https://doi.org/10.1002/2013JD021130, 2014.](#)

1154 [Pisso, I., Sollum, E., Grythe, H., Kristiansen, N., Cassiani, M., Eckhardt, S., Arnold, D., Morton,](#)  
1155 [D., Thompson, R. L., Groot Zwaaftink, C. D., Evangeliou, N., Sodemann, H., Haimberger, L.,](#)  
1156 [Henne, S., Brunner, D., Burkhardt, J. F., Fouilloux, A., Brioude, J., Philipp, A., Seibert, P., and](#)  
1157 [Stohl, A.: The Lagrangian particle dispersion model FLEXPART version 10.4, \*Geosci. Model Dev.\*,](#)  
1158 [12, 4955–4997, <https://doi.org/10.5194/gmd-12-4955-2019>, 2019.](#)

1159 [Pope, C. A. and Dockery, D. W.: Health effects of fine particulate air pollution: Lines that connect,](#)  
1160 [\*J. Air Waste Manag. Assoc.\*, 56, 709–742, <https://doi.org/10.1080/10473289.2006.10464485>, 2006.](#)

1161 [Pope III, C. A., Burnett, R. T., Thun, M. J., Calle, E. E., Krewski, D., and Thurston, G. D.: Lung](#)  
1162 [Cancer, Cardiopulmonary Mortality, and Long-term Exposure to Fine Particulate Air Pollution, \*J.\*](#)  
1163 [Am. Med. Assoc.](#), 287, 1132–1141, <https://doi.org/10.1001/jama.287.9.1132>, 2002.

1164 [Pozzer, A., Tsimpidi, A. P., Karydis, V. A., De Meij, A., and Lelieveld, J.: Impact of agricultural](#)  
1165 [emission reductions on fine-particulate matter and public health, \*Atmos. Chem. Phys.\*, 17, 12813–](#)  
1166 [12826, <https://doi.org/10.5194/acp-17-12813-2017>, 2017.](#)

1167 [Putaud, J. P., Pozzoli, L., Pisoni, E., Martins Dos Santos, S., Lagler, F., Lanzani, G., Dal Santo, U.,](#)  
1168 [and Colette, A.: Impacts of the COVID-19 lockdown on air pollution at regional and urban](#)

1169 [background sites in northern Italy, Atmos. Chem. Phys., 21, 7597–7609,](#)  
1170 <https://doi.org/10.5194/acp-21-7597-2021>, 2021.

1171 [Putaud, J. P., Pisoni, E., Mangold, A., Hueglin, C., Sciare, J., Pikridas, M., Savvides, C., Ondracek,](#)  
1172 [J., Mbengue, S., Wiedensohler, A., Weinhold, K., Merkel, M., Poulain, L., Van Pinxteren, D.,](#)  
1173 [Herrmann, H., Massling, A., Nordstroem, C., Alastuey, A., Reche, C., Pérez, N., Castillo, S.,](#)  
1174 [Sorribas, M., Adame, J. A., Petaja, T., Lehtipalo, K., Niemi, J., Riffault, V., De Brito, J. F., Colette,](#)  
1175 [A., Favez, O., Petit, J. E., Gros, V., Gini, M. I., Vratolis, S., Eleftheriadis, K., Diapouli, E., Denier](#)  
1176 [Van Der Gon, H., Yttri, K. E., and Aas, W.: Impact of 2020 COVID-19 lockdowns on particulate](#)  
1177 [air pollution across Europe, Atmos. Chem. Phys., 23, 10145–10161, https://doi.org/10.5194/acp-23-](#)  
1178 [10145-2023](#), 2023.

1179 [Querol, X., Massagué, J., Alastuey, A., Moreno, T., Gangoiti, G., Mantilla, E., Duéñez, J. J.,](#)  
1180 [Escudero, M., Monfort, E., Pérez García-Pando, C., Petetin, H., Jorba, O., Vázquez, V., de la Rosa,](#)  
1181 [J., Campos, A., Muñóz, M., Monge, S., Hervás, M., Javato, R., and Cornide, M. J.: Lessons from](#)  
1182 [the COVID-19 air pollution decrease in Spain: Now what?, Sci. Total Environ., 779,](#)  
1183 <https://doi.org/10.1016/j.scitotenv.2021.146380>, 2021.

1184 [Reche, C., Viana, M., Pandolfi, M., Alastuey, A., Moreno, T., Amato, F., Ripoll, A., and Querol,](#)  
1185 [X.: Urban NH<sub>3</sub> levels and sources in a Mediterranean environment, Atmos. Environ., 57, 153–164,](#)  
1186 <https://doi.org/10.1016/j.atmosenv.2012.04.021>, 2012.

1187 [Rennie, S., Watkins, J., Ball, L., Brown, M., Fry, M., Henrys, P., Hollaway, M., Quinn, J., Sier, A.,](#)  
1188 [and Dick, J.: Shaping the development of the UKCEH UK-SCAPE Data Science Framework.](#)  
1189 [Workshop report, 2020.](#)

1190 [Rodgers, C. D.: Inverse Methods for Atmospheric Sounding, WORLD SCIENTIFIC, 256 pp.,](#)  
1191 <https://doi.org/doi:10.1142/3171>, 2000.

1192 [Schobesberger, S., Franchin, A., Bianchi, F., Rondo, L., Duplissy, J., Kürten, A., Ortega, I. K.,](#)  
1193 [Metzger, A., Schnitzhofer, R., Almeida, J., Amorim, A., Dommen, J., Dunne, E. M., Ehn, M.,](#)  
1194 [Gagné, S., Ickes, L., Junninen, H., Hansel, A., Kerminen, V. M., Kirkby, J., Kupc, A., Laaksonen,](#)  
1195 [A., Lehtipalo, K., Mathot, S., Onnela, A., Petäjä, T., Riccobono, F., Santos, F. D., Sipilä, M., Tomé,](#)  
1196 [A., Tsagkogeorgas, G., Viisanen, Y., Wagner, P. E., Wimmer, D., Curtius, J., Donahue, N. M.,](#)  
1197 [Baltensperger, U., Kulmala, M., and Worsnop, D. R.: On the composition of ammonia-sulfuric-acid](#)  
1198 [ion clusters during aerosol particle formation, Atmos. Chem. Phys., 15, 55–78,](#)  
1199 <https://doi.org/10.5194/acp-15-55-2015>, 2015.

1200 [Seinfeld, J. H. and Pandis, S. N.: Atmospheric Chemistry and Physics. From Air Pollution to](#)  
1201 [Climate Change, 2nd ed., John Wiley & Sons, NY, 2000.](#)

1202 [Shephard, M. W. and Cady-Pereira, K. E.: Cross-track Infrared Sounder \(CrIS\) satellite](#)  
1203 [observations of tropospheric ammonia, Atmos. Meas. Tech., 8, 1323–1336,](#)

1204 <https://doi.org/10.5194/amt-8-1323-2015>, 2015.

1205 Shephard, M. W., McLinden, C. A., Cady-Pereira, K. E., Luo, M., Moussa, S. G., Leithead, A.,  
1206 Liggio, J., Staebler, R. M., Akingunola, A., Makar, P., Lehr, P., Zhang, J., Henze, D. K., Millet, D.  
1207 B., Bash, J. O., Zhu, L., Wells, K. C., Capps, S. L., Chaliyakunnel, S., Gordon, M., Hayden, K.,  
1208 Brook, J. R., Wolde, M., and Li, S. M.: Tropospheric Emission Spectrometer (TES) satellite  
1209 observations of ammonia, methanol, formic acid, and carbon monoxide over the Canadian oil sands:  
1210 Validation and model evaluation, *Atmos. Meas. Tech.*, 8, 5189–5211, <https://doi.org/10.5194/amt-8-5189-2015>, 2015.

1211 Shephard, M. W., Dammers, E., Cady-Pereira, K., Kharol, S., Thompson, J., Gainariu-Matz,  
1212 Y., Zhang, J., A. McLinden, C., Kovachik, A., Moran, M., Bittman, S., E. Sioris, C., Griffin, D., J.  
1213 Alvarado, M., Lonsdale, C., Savic-Jovicic, V., and Zheng, Q.: Ammonia measurements from space  
1214 with the Cross-track Infrared Sounder: Characteristics and applications. *Atmos. Chem. Phys.*, 20,  
1215 2277–2302, <https://doi.org/10.5194/acp-20-2277-2020>, 2020.

1216 Shi, X. and Brasseur, G. P.: The Response in Air Quality to the Reduction of Chinese Economic  
1217 Activities During the COVID-19 Outbreak, *Geophys. Res. Lett.*, 47, 1–8,  
1218 <https://doi.org/10.1029/2020GL088070>, 2020.

1219 Shi, Z., Song, C., Liu, B., Lu, G., Xu, J., Van Vu, T., Elliott, R. J. R., Li, W., Bloss, W. J., and  
1220 Harrison, R. M.: Abrupt but smaller than expected changes in surface air quality attributable to  
1221 COVID-19 lockdowns, *Sci. Adv.*, 7, <https://doi.org/10.1126/sciadv.abd6696>, 2021.

1222 Sicard, P., De Marco, A., Agathokleous, E., Feng, Z., Xu, X., Paoletti, E., Rodriguez, J. J. D., and  
1223 Calatayud, V.: Amplified ozone pollution in cities during the COVID-19 lockdown, *Sci. Total*  
1224 *Environ.*, 735, <https://doi.org/10.1016/j.scitotenv.2020.139542>, 2020.

1225 Sitwell, M., Shephard, M., Rochon, Y., Cady-Pereira, K., and Dammers, E.: An Ensemble-  
1226 Variational Inversion System for the Estimation of Ammonia Emissions using CrIS Satellite  
1227 Ammonia Retrievals, 22, 6595–6624, <https://doi.org/10.5194/acp-22-6595-2022>, 2022.

1228 Sohrabi, C., Alsafi, Z., O'Neill, N., Khan, M., Kerwan, A., Al-Jabir, A., Iosifidis, C., and Agha, R.:  
1229 World Health Organization declares global emergency: A review of the 2019 novel coronavirus  
1230 (COVID-19), *Int. J. Surg.*, 76, 71–76, <https://doi.org/10.1016/j.ijisu.2020.02.034>, 2020.

1231 Sørensen, L. L., Hertel, O., Skjøth, C. A., Lund, M., and Pedersen, B.: Fluxes of ammonia in the  
1232 coastal marine boundary layer, *Atmos. Environ.*, 37, 167–177, [https://doi.org/10.1016/S1352-2310\(03\)00247-4](https://doi.org/10.1016/S1352-2310(03)00247-4), 2003.

1233 Stevens, C. J., Dupr, C., Dorland, E., Gaudnik, C., Gowing, D. J. G., Bleeker, A., Diekmann, M.,  
1234 Alard, D., Bobbink, R., Fowler, D., Corcket, E., Mountford, J. O., Vandvik, V., Aarrestad, P. A.,  
1235 Muller, S., and Dise, N. B.: Nitrogen deposition threatens species richness of grasslands across  
1236 Europe, *Environ. Pollut.*, 158, 2940–2945, <https://doi.org/10.1016/j.envpol.2010.06.006>, 2010.

1239 [Stohl, A., Forster, C., Frank, A., Seibert, P., and Wotawa, G.: Technical note: The Lagrangian](#)  
1240 [particle dispersion model FLEXPART version 6.2, Atmos. Chem. Phys., 5, 2461–2474,](#)  
1241 <https://doi.org/10.5194/acp-5-2461-2005>, 2005.

1242 [Sutton, M. A., Dragosits, U., Tang, Y. S., and Fowler, D.: Ammonia emissions from non-](#)  
1243 [agricultural sources in the UK, 34, 2000a.](#)

1244 [Sutton, M. A., Dragosits, U., Tang, Y. S., and Fowler, D.: Ammonia emissions from non-](#)  
1245 [agricultural sources in the UK, Atmos. Environ., 34, 855–869, 2000b.](#)

1246 [Sutton, M. A., Erisman, J. W., Dentener, F., and Möller, D.: Ammonia in the environment: From](#)  
1247 [ancient times to the present, Environ. Pollut., 156, 583–604,](#)  
1248 <https://doi.org/10.1016/j.envpol.2008.03.013>, 2008.

1249 [Sutton, M. A., Reis, S., Riddick, S. N., Dragosits, U., Nemitz, E., Theobald, M. R., Tang, Y. S.,](#)  
1250 [Braban, C. F., Vieno, M., Dore, A. J., Mitchell, R. F., Wanless, S., Daunt, F., Fowler, D., Blackall,](#)  
1251 [T. D., Milford, C., Flechard, C. R., Loubet, B., Massad, R., Cellier, P., Personne, E., Coheur, P. F.,](#)  
1252 [Clarisse, L., Damme, M. Van, Ngadi, Y., Clerbaux, C., Skjøth, C. A., Geels, C., Hertel, O., Kruit,](#)  
1253 [R. J. W., Pinder, R. W., Bash, J. O., Walker, J. T., Simpson, D., Horvath, L., Misselbrook, T. H.,](#)  
1254 [Bleeker, A., Dentener, F., and Vries, W. de: Towards a climate-dependent paradigm of ammonia](#)  
1255 [emission and deposition, Philos. Trans. R. Soc. B Biol. Sci., 368, 20130166–20130166,](#)  
1256 <https://doi.org/10.1098/rstb.2013.0166>, 2013.

1257 [Szczepańska, A. and Pietrzyka, K.: The COVID-19 epidemic in Poland and its influence on the](#)  
1258 [quality of life of university students \(young adults\) in the context of restricted access to public](#)  
1259 [spaces, J. Public Heal., https://doi.org/10.1007/s10389-020-01456-z](#), 2021.

1260 [Thunis, P., Clappier, A., Beekmann, M., Putaud, J. P., Cuvelier, C., Madrazo, J., and De Meij, A.:](#)  
1261 [Non-linear response of PM<sub>2.5</sub> to changes in NO<sub>x</sub> and NH<sub>3</sub> emissions in the Po basin \(Italy\):](#)  
1262 [Consequences for air quality plans, Atmos. Chem. Phys., 21, 9309–9327,](#)  
1263 <https://doi.org/10.5194/acp-21-9309-2021>, 2021.

1264 [Tichý, O., Šmídl, V., Hofman, R., and Stohl, A.: LS-APC v1.0: A tuning-free method for the linear](#)  
1265 [inverse problem and its application to source-Term determination, Geosci. Model Dev., 9, 4297–](#)  
1266 [4311, https://doi.org/10.5194/gmd-9-4297-2016](#), 2016.

1267 [Tichý, O., Ulrych, L., Šmídl, V., Evangelidou, N., and Stohl, A.: On the tuning of atmospheric](#)  
1268 [inverse methods: Comparisons with the European Tracer Experiment \(ETEX\) and Chernobyl](#)  
1269 [datasets using the atmospheric transport model FLEXPART, Geosci. Model Dev., 13, 5917–5934,](#)  
1270 <https://doi.org/10.5194/gmd-13-5917-2020>, 2020.

1271 [Tichý, O., Eckhardt, S., Balkanski, Y., Hauglustaine, D., and Evangelidou, N.: Decreasing trends of](#)  
1272 [ammonia emissions over Europe seen from remote sensing and inverse modelling, Atmos. Chem.](#)  
1273 [Phys., 23, 15235–15252, https://doi.org/10.5194/acp-23-15235-2023](#), 2023.

1274 [Varotsos, C., Christodoulakis, J., Kouremadas, G. A., and Fotaki, E. F.: The Signature of the](#)  
1275 [Coronavirus Lockdown in Air Pollution in Greece, \*Water, Air, Soil Pollut.\*, 232,](#)  
1276 <https://doi.org/10.1007/s11270-021-05055-w>, 2021.  
1277 [Viatte, C., Petit, J. E., Yamanouchi, S., Van Damme, M., Doucerain, C., Germain-Piaulenne, E.,](#)  
1278 [Gros, V., Favez, O., Clarisse, L., Coheur, P. F., Strong, K., and Clerbaux, C.: Ammonia and pm2.5](#)  
1279 [air pollution in paris during the 2020 covid lockdown, \*Atmosphere \(Basel\)\*, 12, 1–18,](#)  
1280 <https://doi.org/10.3390/atmos12020160>, 2021.  
1281 [De Vries, W., Kros, J., Reinds, G. J., and Butterbach-Bahl, K.: Quantifying impacts of nitrogen use](#)  
1282 [in European agriculture on global warming potential, \*Curr. Opin. Environ. Sustain.\*, 3, 291–302,](#)  
1283 <https://doi.org/10.1016/j.cosust.2011.08.009>, 2011.  
1284 [Walters, W. W., Chai, J., and Hastings, M. G.: Theoretical Phase Resolved Ammonia-Ammonium](#)  
1285 [Nitrogen Equilibrium Isotope Exchange Fractionations: Applications for Tracking Atmospheric](#)  
1286 [Ammonia Gas-to-Particle Conversion, \*ACS Earth Sp. Chem.\*, 3, 79–89,](#)  
1287 <https://doi.org/10.1021/acsearthspacechem.8b00140>, 2019.  
1288 [Wang, M., Xiao, M., Bertozzi, B., Marie, G., Rörup, B., Schulze, B., Bardakov, R., He, X. C., Shen,](#)  
1289 [J., Scholz, W., Marten, R., Dada, L., Baalbaki, R., Lopez, B., Lamkaddam, H., Manninen, H. E.,](#)  
1290 [Amorim, A., Ataei, F., Bogert, P., Brasseur, Z., Caudillo, L., De Menezes, L. P., Duplissy, J.,](#)  
1291 [Ekman, A. M. L., Finkenzeller, H., Carracedo, L. G., Granzin, M., Guida, R., Heinritzi, M.,](#)  
1292 [Hofbauer, V., Höhler, K., Korhonen, K., Krechmer, J. E., Kürten, A., Lehtipalo, K., Mahfouz, N. G.](#)  
1293 [A., Makhmutov, V., Massabò, D., Mathot, S., Mauldin, R. L., Mentler, B., Müller, T., Onnela, A.,](#)  
1294 [Petäjä, T., Philippov, M., Piedehierro, A. A., Pozzer, A., Ranjithkumar, A., Schervish, M.,](#)  
1295 [Schobesberger, S., Simon, M., Stozhkov, Y., Tomé, A., Umo, N. S., Vogel, F., Wagner, R., Wang,](#)  
1296 [D. S., Weber, S. K., Welti, A., Wu, Y., Zauner-Wieczorek, M., Sipilä, M., Winkler, P. M., Hansel,](#)  
1297 [A., Baltensperger, U., Kulmala, M., Flagan, R. C., Curtius, J., Riipinen, I., Gordon, H., Lelieveld,](#)  
1298 [J., El-Haddad, I., Volkamer, R., Worsnop, D. R., Christoudias, T., Kirkby, J., Möhler, O., and](#)  
1299 [Donahue, N. M.: Synergistic HNO<sub>3</sub>–H<sub>2</sub>SO<sub>4</sub>–NH<sub>3</sub> upper tropospheric particle formation, \*Nature\*,](#)  
1300 [605, 483–489, https://doi.org/10.1038/s41586-022-04605-4](#), 2022.  
1301 [Wang, P., Chen, K., Zhu, S., Wang, P., and Zhang, H.: Severe air pollution events not avoided by](#)  
1302 [reduced anthropogenic activities during COVID-19 outbreak, \*Resour. Conserv. Recycl.\*, 158,](#)  
1303 [104814, https://doi.org/10.1016/j.resconrec.2020.104814](https://doi.org/10.1016/j.resconrec.2020.104814), 2020.  
1304 [Weber, R. J., McMurry, P. H., Mauldin, R. L., Tanner, D. J., Eisele, F. L., Clarke, A. D., and](#)  
1305 [Kapustin, V. N.: New particle formation in the remote troposphere: A comparison of observations](#)  
1306 [at various sites, \*Geophys. Res. Lett.\*, 26, 307–310, https://doi.org/10.1029/1998GL900308](#), 1999.  
1307 [White, E., Shephard, M. W., Cady-Pereira, K. E., Kharol, S. K., Ford, S., Dammers, E., Chow, E.,](#)  
1308 [Thiessen, N., Tobin, D., Quinn, G., O'Brien, J., and Bash, J.: Accounting for Non-Detects:](#)



1309 [Application to Satellite Ammonia Observations, Remote Sens., 15,](#)  
1310 <https://doi.org/10.3390/rs15102610>, 2023.

1311 [Xu, W., Zhao, Y., Wen, Z., Chang, Y., Pan, Y., Sun, Y., and Ma, X.: Increasing importance of](#)  
1312 [ammonia emission abatement in PM2.5 pollution control, Sci. Bull., 67, 1745–1749,](#)  
1313 <https://doi.org/10.1016/j.scib.2022.07.021>, 2022.

1314 [Zavyalov, V., Esplin, M., Scott, D., Esplin, B., Bingham, G., Hoffman, E., Lietzke, C., Predina, J.,](#)  
1315 [Frain, R., Suwinski, L., Han, Y., Major, C., Graham, B., and Phillips, L.: Noise performance of the](#)  
1316 [CrIS instrument, J. Geophys. Res. Atmos., 118, 108–120, https://doi.org/10.1002/2013JD020457,](#)  
1317 [2013.](#)

1318 [Zhai, S., Jacob, D. J., Wang, X., Liu, Z., Wen, T., Shah, V., Li, K., Moch, J. M., Bates, K. H., Song,](#)  
1319 [S., Shen, L., Zhang, Y., Luo, G., Yu, F., Sun, Y., Wang, L., Qi, M., Tao, J., Gui, K., Xu, H., Zhang,](#)  
1320 [Q., Zhao, T., Wang, Y., Lee, H. C., Choi, H., and Liao, H.: Control of particulate nitrate air](#)  
1321 [pollution in China, Nat. Geosci., 14, 389–395, https://doi.org/10.1038/s41561-021-00726-z](#), 2021.

1322 [Zhang, X., Zhang, Z., Xiao, Z., Tang, G., Li, H., Gao, R., Dao, X., Wang, Y., and Wang, W.: Heavy](#)  
1323 [haze pollution during the COVID-19 lockdown in the Beijing-Tianjin-Hebei region, China, J.](#)  
1324 [Environ. Sci. \(China\), 114, 170–178, https://doi.org/10.1016/j.jes.2021.08.030](#), 2022.

1325 [Zhang, Y., Zhang, C., Liu, Z., and Yang, X.: Air pollution reduction during COVID-19 lockdown](#)  
1326 [in China: a sustainable impact assessment for future cities development, City Built Environ., 1, 1–](#)  
1327 [21, https://doi.org/10.1007/s44213-023-00013-0](#), 2023.

1328

1329

Formatted: Font: (Default) Times New Roman, 12 pt

**Deleted:** Abbatt, J. P. D., Benz, S., Cziczo, D. J., Kanji, Z., Lohmann, U., and Mohler, O.: Solid Ammonium Sulfate Aerosols as Ice Nuclei: A Pathway for Cirrus Cloud Formation, *Science* (80-. ), 313, 1770–1773, 2006. [¶](#)

Acharya, P., Barik, G., Gayen, B. K., Bar, S., Maiti, A., Sarkar, A., Ghosh, S., De, S. K., and Sreekesh, S.: Revisiting the levels of Aerosol Optical Depth in south-southeast Asia, Europe and USA amid the COVID-19 pandemic using satellite observations, *Environ. Res.*, 193, 110514, <https://doi.org/10.1016/j.envres.2020.110514>, 2021. [¶](#)

Anderson, N., Strader, R., and Davidson, C.: Airborne reduced nitrogen: Ammonia emissions from agriculture and other sources, *Environ. Int.*, 29, 277–286, [https://doi.org/10.1016/S0160-4120\(02\)00186-1](https://doi.org/10.1016/S0160-4120(02)00186-1), 2003. [¶](#)

Archer, C. L., Cervone, G., Golbazi, M., Al Fahel, N., and Hultquist, C.: Changes in air quality and human mobility in the USA during the COVID-19 pandemic, *Bull. Atmos. Sci. Technol.*, 1, 491–514, <https://doi.org/10.1007/s42865-020-00019-0>, 2020. [¶](#)

Baekgaard, M., Christensen, J., Madsen, J. K., and Mikkelsen, K. S.: Rallying around the flag in times of COVID-19: Societal lockdown and trust in democratic institutions, *J. Behav. Public Adm.*, 3, 1–12, <https://doi.org/10.30636/jbpa.32.172>, 2020. [¶](#)

Bauwens, M., Compennolle, S., Stavrakou, T., Müller, J. F., van Gent, J., Eskes, H., Levelt, P. F., van der A, R., Veeckind, J. P., Vlietinck, J., Yu, H., and Zehner, C.: Impact of Coronavirus Outbreak on NO2 Pollution Assessed Using TROPOMI and OMI Observations, *Geophys. Res. Lett.*, 47, 1–9, <https://doi.org/10.1029/2020GL087978>, 2020. [¶](#)

Bekbulat, B., Apte, J. S., Millet, D. B., Robinson, A. L., Wells, K. C., Presto, A. A., and Marshall, J. D.: Changes in criteria air pollution levels in the US before, during, and after Covid-19 stay-at-home orders: Evidence from regulatory monitors, *Sci. Total Environ.*, 769, 144693, <https://doi.org/10.1016/j.scitotenv.2020.144693>, 2021. [¶](#)

Bellouin, N., Rae, J., Jones, A., Johnson, C., Haywood, J., and Boucher, O.: Aerosol forcing in the Climate Model Intercomparison Project (CMIP5) simulations by HadGEM2-ES and the role of ammonium nitrate, *J. Geophys. Res. Atmos.*, 116, 1–25, <https://doi.org/10.1029/2011JD016074>, 2011. [¶](#)

Bendz, B. and Aaberge, L.: COVID-19 spread in the UK: the end of the beginning?, *Lancet*, 396, 587–590, [https://doi.org/https://doi.org/10.1016/S0140-6736\(20\)31689-5](https://doi.org/https://doi.org/10.1016/S0140-6736(20)31689-5) www.thelancet.com, 2020. [¶](#)

Bouwman, A. F., Lee, D. S., Asman, W. A. H., Dentener, F. J., Van Der Hoek, K. W., and Olivier, J. G. J.: A global high-resolution emission inventory for ammonia, *Global Biogeochem. Cycles*, 11, 561–587, <https://doi.org/10.1029/97GB02266>, 1997. [¶](#)

Bressi, M., Sciare, J., Ghersi, V., Bonnair, N., Nicolas, J. B., Petit, J. E., Moukhtar, S., Rosso, A., Mihalopoulos, N., and Féron, A.: A one-year comprehensive chemical characterisation of fine aerosol (PM2.5) at urban, suburban and rural background sites in the region of Paris (France), *Atmos. Chem. Phys.*, 13, 7825–7844, <https://doi.org/10.5194/acp-13-7825-2013>, 2013. [¶](#)

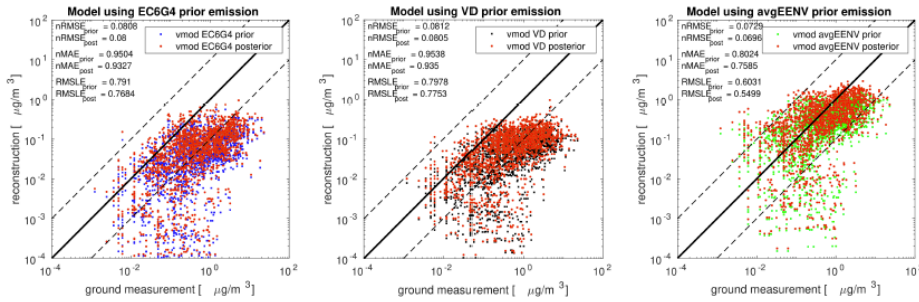
Camargo, J. A. and Alonso, Á.: Ecological and toxicological effects of inorganic nitrogen pollution in aquatic ecosystems: A global assessment, *Environ. Int.*, 32, 831–849, <https://doi.org/10.1016/j.envint.2006.05.002>, 2006. [¶](#)

Cao, H., Henze, D. K., Shephard, M. W., Dammers, E., Cady-Pereira, K., Alvarado, M., Lonsdale, C., Luo, G., Yu, F., Zhu, L., Danielson, C. G., and Edgerton, E. S.: Inverse modeling of NH3 sources using CrIS remote sensing measurements, *Environ. Res. Lett.*, 15, 104082, <https://doi.org/10.1088/1748-9326/abb5cc>, 2020. [¶](#)

... [3]

1479 **FIGURE LEGENDS**

1480

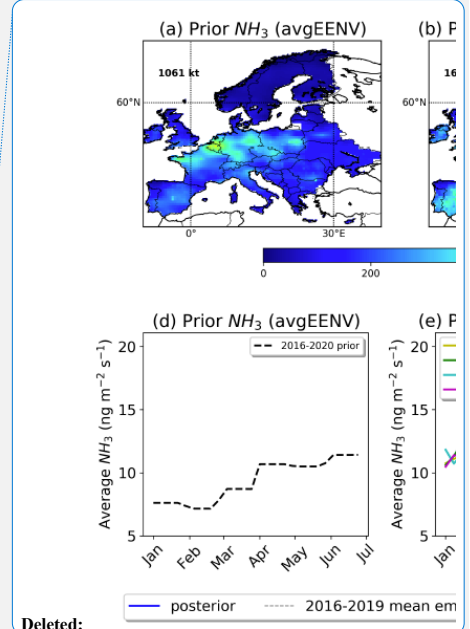
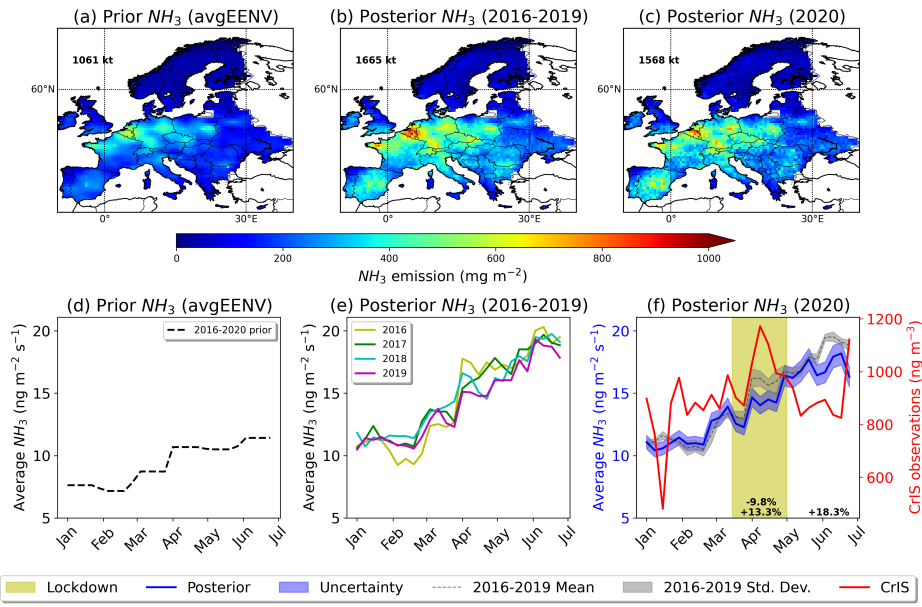


1481

1482 **Figure 1.** Scatter plots of prior and posterior concentrations against independent observations  
1483 (observations that were not included in the inversion algorithm) from the EMEP network  
1484 (<https://emep.int/mscw/>, **Figure S 1**) from January to July 2020. Three statistical measures  
1485 (nRMSE, nMAE and RMSLE) were used to assess the performance of each inversion using three  
1486 different prior emission inventories for ammonia (EC6G4, VD and avgEENV).

1487

Deleted:  
Deleted: Error! Reference source not found.



Deleted:

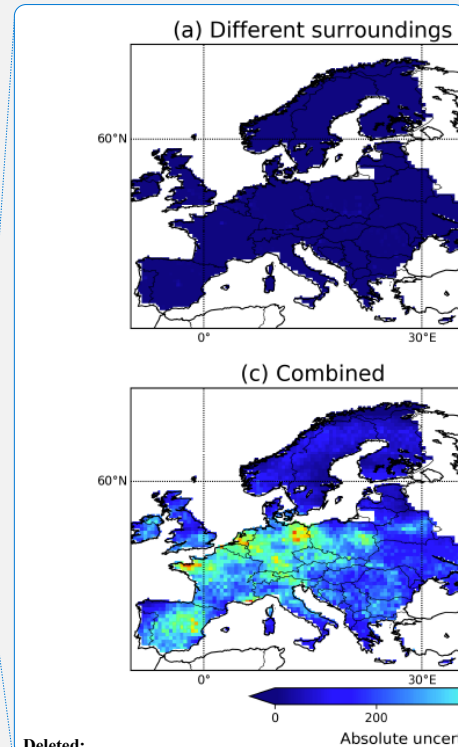
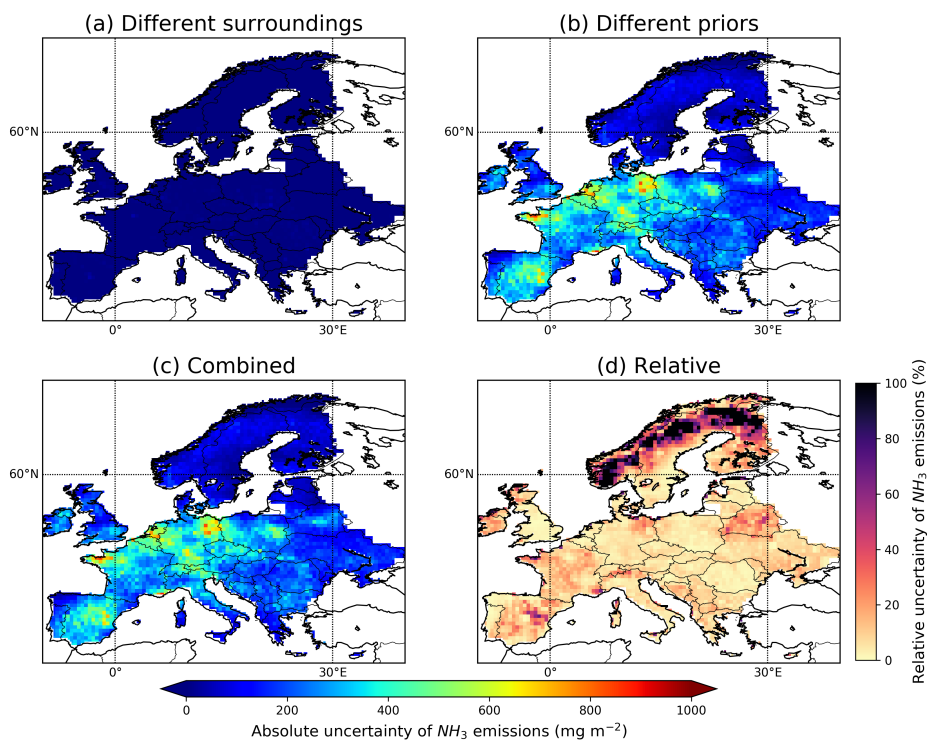
- Deleted: minimum,
- Deleted: and maximum
- Deleted: in

1490

1491 **Figure 2.** (a) Total a priori emissions of ammonia over Europe for the inversion period (January –  
 1492 June). The emissions correspond to avgEENV prior, and the total emitted amount is equal to 1061 kt.  
 1493 (b) Total a posteriori emissions of ammonia over Europe for the inversion period (January – June)  
 1494 for the reference period 2016 – 2019 (using avgEENV prior) that amount 1665 kt. (c) Total posterior  
 1495 emissions of ammonia over Europe for January – June 2020 (1568 kt) using the avgEENV as the  
 1496 prior. (d) Timeseries of weekly-average prior emissions of ammonia over Europe (January to June  
 1497 2020) from avgEENV prior. (e) Timeseries of weekly-average posterior emissions of ammonia over  
 1498 Europe for the reference years 2016–2019 (January to June) (yellow, green, cyan, magenta colors).  
 1499 (f) Timeseries of weekly-average posterior emissions of ammonia with the associated uncertainties  
 1500 over Europe in 2020 resulting from inversions using the avgEENV prior are plotted together with the  
 1501 CrIS observations averaged over Europe (red line) and the mean ammonia emissions with the  
 1502 calculated standard deviations for the reference period (2016–2019). The single top number -9.8%  
 1503 shows percentage change in ammonia emissions during the 2020 lockdown as compared to the same  
 1504 period in reference years, whereas two bottom ones show the corresponding changes in ammonia  
 1505 emissions (i) during the 2020 lockdown as compared to the period before lockdown (+13.3%), and  
 1506 (ii) the period after lockdown finished as compared to the lockdown period +18.3%), known as  
 1507 rebound period.

1508

1509



**Deleted:**

**Formatted:** Keep with next

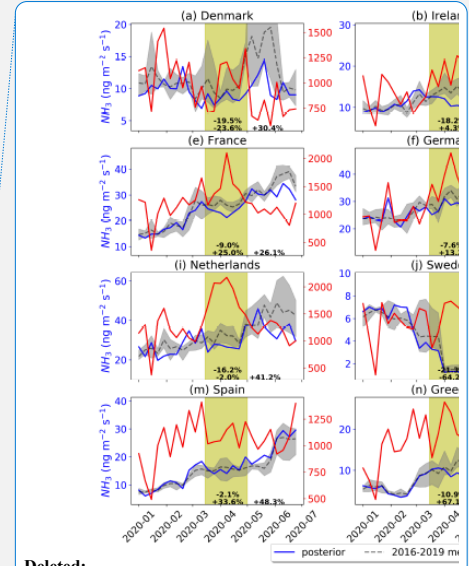
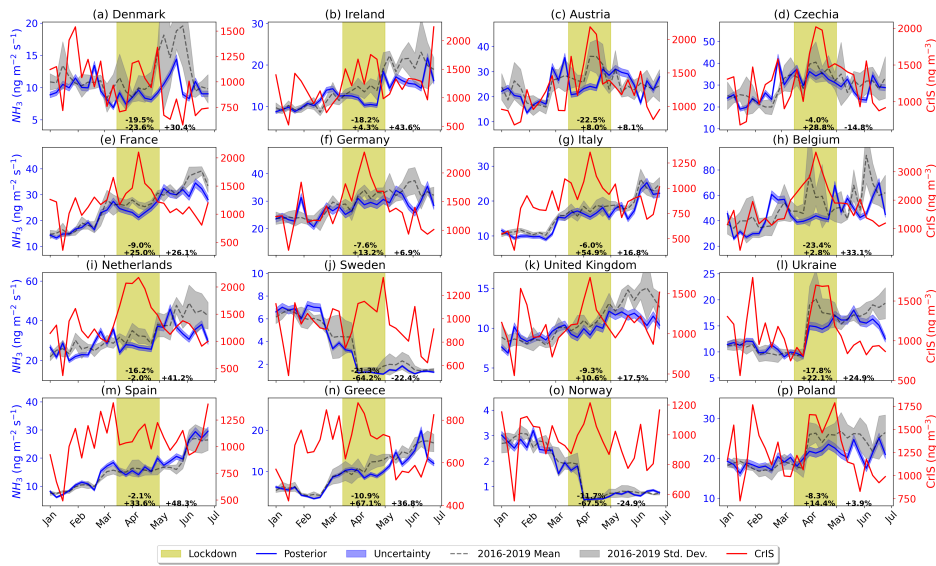
**Formatted:** Font: (Default) Times New Roman, 12 pt, Bold, Not Italic

**Formatted:** Font: (Default) Times New Roman, 12 pt, Bold, Not Italic

**Formatted:** Font: Bold

**Formatted:** Justified

**Deleted:** Figure 5. (a) Absolute uncertainty from use of different surrounding grid area for each spatial element of our inversion domain in the sensitivity tests;  $2^\circ$  to  $4^\circ$  grid-cells were considered resulting in a mean relative uncertainty of 4%. (b) Absolute uncertainty from use of four different prior emission estimates, namely EC6G4, VD, EGG and NE (see section 2.3). Here, a much larger uncertainty was calculated, due to the use of tenfold different prior emission datasets. (c) Propagated absolute uncertainty from the different sensitivity tests, and (d) relative uncertainty with respect to the posterior emissions (Figure 2c). The average uncertainty in the inversion domain for the first half of 2020 was estimated to be 48%.



Deleted:

Deleted: minimum,

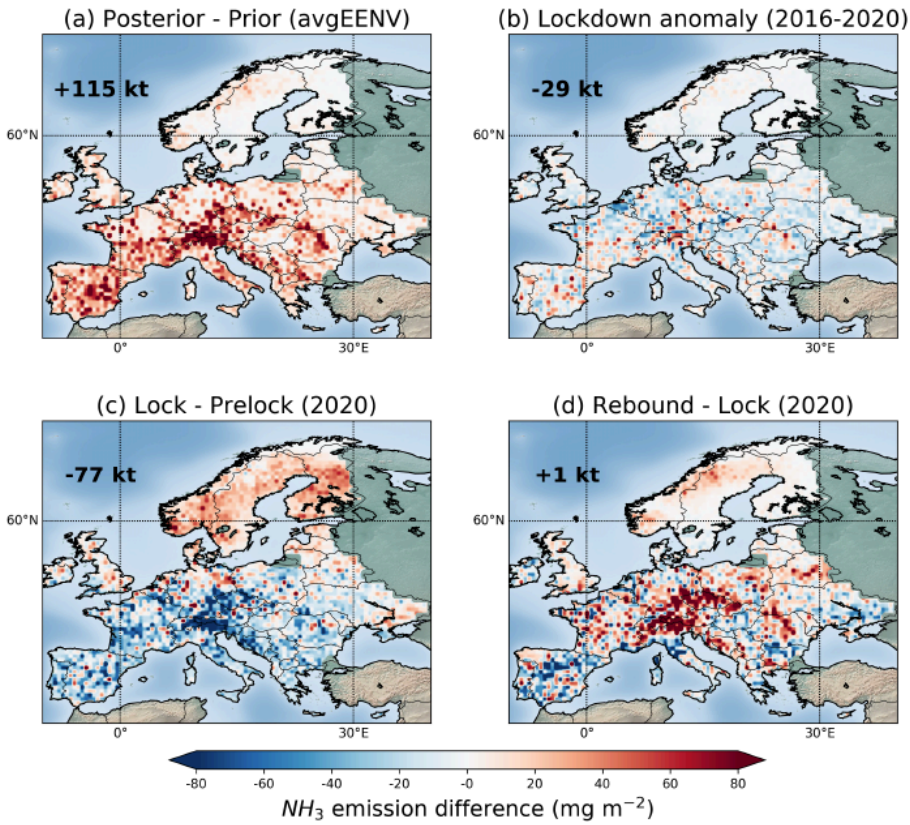
Deleted: and maximum ammonia

1538

1539 **Figure 4.** Timeseries of weekly-average posterior emissions of ammonia with the calculated  
 1540 uncertainties in different European countries in 2020 resulting from inversions using prior  
 1541 information from avgEENV plotted together with the CrIS observations averaged over Europe (red  
 1542 line) and mean emissions with the calculated standard deviations for the reference period (2016–  
 1543 2019). The single top numbers show the change in ammonia emissions during the 2020 lockdowns  
 1544 (15 March – 30 April) as compared to the same period the years before (2016–2019), whereas the two  
 1545 bottom ones show the respective changes in ammonia emissions during the 2020 lockdown as  
 1546 compared to the period before the lockdown, and after lockdown finished compared to the lockdown  
 1547 period (rebound period).

1548

1549

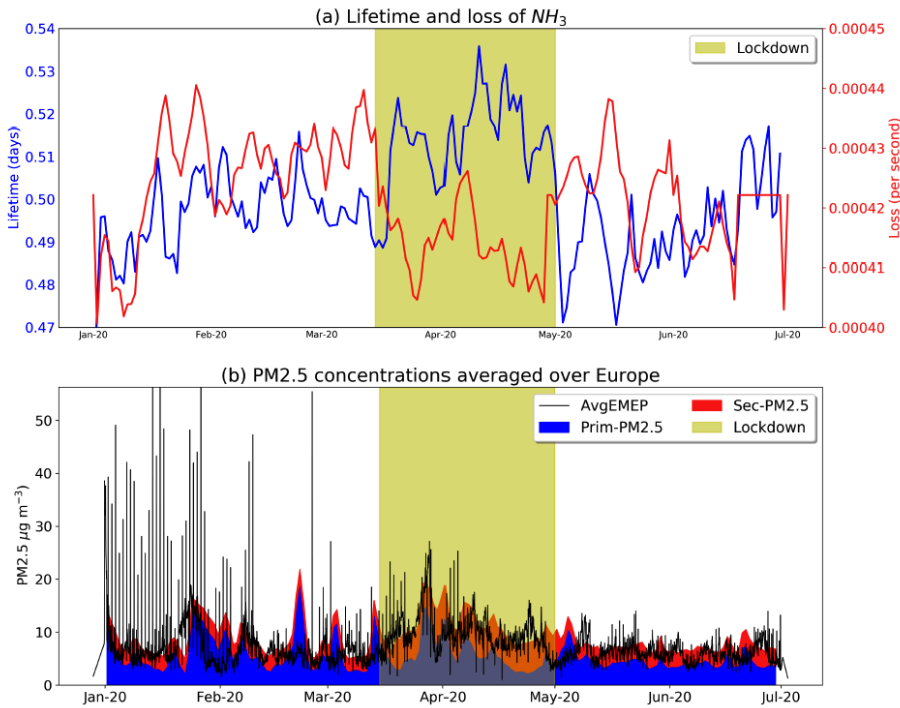


1553

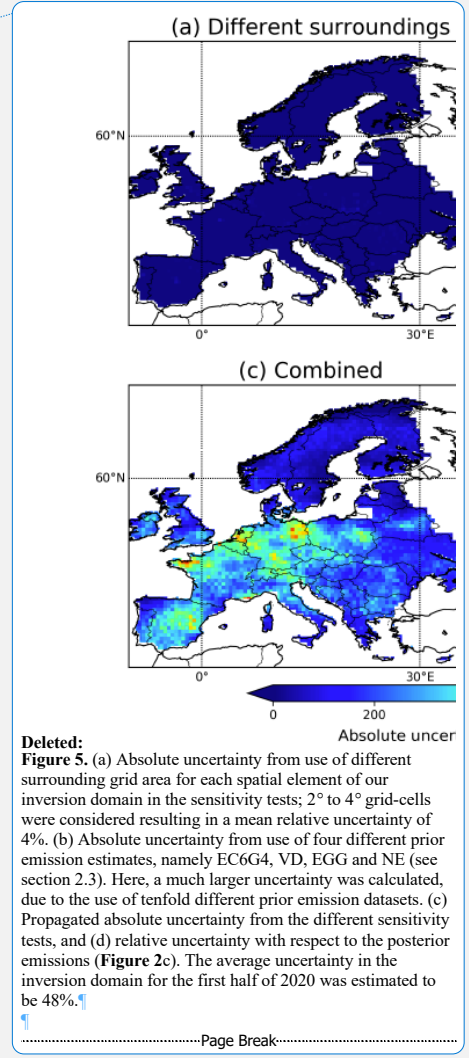
1554 **Figure 5.** (a) Difference of posterior from prior emissions of ammonia during the European  
 1555 lockdowns of 2020 (15 March – 30 April) using the avgEENV emissions as the prior. (b) Emission  
 1556 anomaly relative to the 2020 lockdowns from the 2016-2020 period (15 March – 30 April).  
 1557 Difference in posterior ammonia (c) during the 2020 lockdowns (15 March – 30 April, Lock) from  
 1558 the period before (1 January – 14 March) and (d) after the 2020 lockdowns (1 May – 31 June, Reb)  
 1559 from the period during the 2020 lockdowns (15 March – 30 April, Lock) compared with the  
 1560 reference years (2016–2019).

1561

1562



1565 **Figure 6.** (a) Modelled lifetime (blue) and loss-rates (red) of atmospheric ammonia averaged over  
 1566 Europe for January – June 2020. The lockdown period (15 March – 30 April) is shaded in yellow.  
 1567 Right after COVID-19 restrictions were applied, loss-rates of ammonia (shown in red) were  
 1568 disturbed due to reported decreases on  $SO_2$  and  $NO_x$  (Guevara et al., 2021; Doumbia et al., 2021),  
 1569 precursors of sulfuric and nitric acids (with which ammonia reacts to form PM2.5) and the constant  
 1570 accumulation of atmospheric ammonia. This had an effect on the lifetime of ammonia (plotted in  
 1571 blue), which started increasing in Europe leading to further accumulation of ammonia. (b)  
 1572 Observations of PM2.5 from the EMEP stations (78 stations) plotted against modelled PM2.5  
 1573 concentrations, both averaged over Europe, from primary sources and secondary formation. It is  
 1574 evident that right after lockdown (yellow shade), secondary PM2.5 formation maintained high  
 1575 concentrations across Europe.



~~Deleted:~~  
**Figure 5.** (a) Absolute uncertainty from use of different surrounding grid area for each spatial element of our inversion domain in the sensitivity tests; 2° to 4° grid-cells were considered resulting in a mean relative uncertainty of 4%. (b) Absolute uncertainty from use of four different prior emission estimates, namely EC6G4, VD, EGG and NE (see section 2.3). Here, a much larger uncertainty was calculated, due to the use of tenfold different prior emission datasets. (c) Propagated absolute uncertainty from the different sensitivity tests, and (d) relative uncertainty with respect to the posterior emissions (Figure 2c). The average uncertainty in the inversion domain for the first half of 2020 was estimated to be 48%.  
 .....Page Break.....

1593 **SUPPLEMENTARY FIGURE LEGENDS**

1594  
1595

1596 **Figure S 1.** The EMEP stations (<https://emep.int/mscw/>) providing weekly or bi-weekly ground-  
1597 based observations of ammonia. The highlighted stations were selected to show timeseries of the  
1598 comparison of prior and posterior ammonia against observations.

1599

1600 **Figure S 2.** (a) Total a priori emissions of ammonia over Europe for the inversion period (January –  
1601 June) using EC6G4 as the prior. The total emitted amount is equal to 202 kt. (b) Total a posteriori  
1602 emissions of ammonia over Europe for the reference period (January – June). The emissions are an  
1603 average of respective inversions for years 2016 – 2019 and amount 312 kt. (c) Total posterior  
1604 emissions of ammonia over Europe for January – June 2020 (283 kt). (d). Timeseries of weekly-  
1605 average prior emissions of ammonia over Europe (January to June) from EC6G4. (e) Timeseries of  
1606 weekly-average posterior emissions of ammonia over Europe for years 2016–2019 (January to  
1607 June). (f) Timeseries of weekly-average posterior emissions of ammonia over Europe in 2020  
1608 (January – June). Ammonia emissions during the 2020 lockdown as compared to the same period  
1609 the years before dropped -12.3%. Changes in ammonia emissions during the 2020 lockdown as  
1610 compared to the period before lockdown were -18.2% and rebounded after the end of the lockdown  
1611 (-5.6%).

1612

1613 **Figure S 3.** (a) Total a priori emissions of ammonia over Europe for the inversion period (January –  
1614 June) using VD as the prior. The total emitted amount is equal to 188 kt. (b) Total a posteriori  
1615 emissions of ammonia over Europe for the reference period (January – June). The emissions are an  
1616 average of respective inversions for years 2016 – 2019 and amount 293 kt. (c) Total posterior  
1617 emissions of ammonia over Europe for January – June 2020 (273 kt). (d). Timeseries of weekly-  
1618 average prior emissions of ammonia over Europe (January to June) from VD. (e) Timeseries of  
1619 weekly-average posterior emissions of ammonia over Europe for years 2016–2019 (January to  
1620 June). (f) Timeseries of weekly-average posterior emissions of ammonia over Europe in 2020  
1621 (January – June). Ammonia emissions during the 2020 lockdown as compared to the same period  
1622 the years before dropped by -11.0%. Changes in ammonia emissions during the 2020 lockdown as  
1623 compared to the period before lockdown were -7.9% and rebounded after the end of the lockdown  
1624 (+18.1%).

1625

1626 **Figure S 4.** Average surface temperature, specific humidity and precipitation over Europe from  
1627 January to June for the years 2016-2020 from ECMWF ERA5 (Hersbach et al., 2020). Temperature,  
1628 humidity and precipitation are not significantly different than any of the previous years and cannot  
1629 justify more volatilisation of ammonia. This is additional evidence that the impact from  
1630 meteorology did not drive ammonia or PM2.5 formation. The lockdown period is shaded in grey.

Formatted: Font: (Default) Times New Roman, 12 pt, Bold, Not Italic, Font colour: Text 1, English (UK)

Formatted: Caption

Formatted: Font: Not Bold, Font colour: Text 1

1631

1632 **Figure S 5.** Timeseries of prior and posterior ammonia against observations from eight EMEP sites.  
1633 In most cases better statistics were obtained with respect to RMSEs and MAEs.

1634

1635 **Figure S 6.** Country masks used to calculate emissions of ammonia over different European  
1636 countries, namely Austria, Belgium, Denmark, Finland, France, Germany, Greece, Iceland, Ireland,  
1637 Italy, Luxembourg, Netherlands, Norway, Portugal, Spain, Sweden, Switzerland, Turkey, United  
1638 Kingdom, Albania, Belarus, Bosnia and Herzegovina, Bulgaria, Croatia, Cyprus, Czechia, Estonia,  
1639 Hungary, Latvia, Lithuania, Malta, Poland, Republic of Moldova, Romania, Slovakia, Slovenia,  
1640 North Macedonia, Ukraine, Serbia (Russian Federation was excluded from the study).



1641

1642 **Figure S 7.** Modelled concentrations of PM<sub>2.5</sub> against ground-based observations from EMEP  
1643 stations for January to June 2020 presented in a Taylor diagram. The diagram shows the Pearson's  
1644 correlation coefficient (gauging similarity in pattern between the modelled and observed  
1645 concentrations) that is related to the azimuthal angle (blue contours); the standard deviation of  
1646 modelled concentrations of ammonia is proportional to the radial distance from the origin (black  
1647 contours) and the centered normalized RMSE of modelled concentrations is proportional to the  
1648 distance from the reference standard deviation (green contours).

1649

1650 **Figure S 8.** Temperature (red) and specific humidity (blue) spatially averaged over Europe and  
1651 vertically averaged up to 32 km (795 mbars) from ERA5 (Hersbach et al., 2020) for January – June  
1652 2020. The lockdown period is shaded in grey.